

UC Berkeley

UC Berkeley Previously Published Works

Title

Measurement of angular and momentum distributions of charged particles within and around jets in Pb+Pb and pp collisions at $\sqrt{s_{NN}}=5.02$ TeV with the ATLAS detector

Permalink

<https://escholarship.org/uc/item/9z0193s3>

Journal

Physical Review C, 100(6)

ISSN

2469-9985

Authors

Aad, G

Abbott, B

Abbott, DC

et al.

Publication Date

2020-01-13


DOI

10.1103/physrevc.100.064901

Peer reviewed

Measurement of angular and momentum distributions of charged particles within and around jets in Pb + Pb and pp collisions at $\sqrt{s_{NN}} = 5.02$ TeV with the ATLAS detector

G. Aad *et al.**
(ATLAS Collaboration)

 (Received 17 August 2019; published 2 December 2019)

Studies of the fragmentation of jets into charged particles in heavy-ion collisions can provide information about the mechanism of jet quenching by the hot and dense QCD matter created in such collisions, the quark-gluon plasma. This paper presents a measurement of the angular distribution of charged particles around the jet axis in $\sqrt{s_{NN}} = 5.02$ TeV Pb + Pb and pp collisions, using the ATLAS detector at the LHC. The Pb + Pb and pp data sets have integrated luminosities of 0.49 nb^{-1} and 25 pb^{-1} , respectively. The measurement is performed for jets reconstructed with the anti- k_t algorithm with radius parameter $R = 0.4$ and is extended to an angular distance of $r = 0.8$ from the jet axis. Results are presented as a function of Pb + Pb collision centrality and distance from the jet axis for charged particles with transverse momenta in the 1- to 63-GeV range, matched to jets with transverse momenta in the 126- to 316-GeV range and an absolute value of jet rapidity of less than 1.7. Modifications to the measured distributions are quantified by taking a ratio to the measurements in pp collisions. Yields of charged particles with transverse momenta below 4 GeV are observed to be increasingly enhanced as a function of angular distance from the jet axis, reaching a maximum at $r = 0.6$. Charged particles with transverse momenta above 4 GeV have an enhanced yield in Pb + Pb collisions in the jet core for angular distances up to $r = 0.05$ from the jet axis, with a suppression at larger distances.

DOI: [10.1103/PhysRevC.100.064901](https://doi.org/10.1103/PhysRevC.100.064901)

I. INTRODUCTION

Ultrarelativistic nuclear collisions at the Large Hadron Collider (LHC) produce hot, dense matter called a quark-gluon plasma, QGP (see Refs. [1,2] for recent reviews). Jets from hard-scattering processes in these collisions traverse and interact with the QGP, losing energy via a process called jet quenching. The rates and characteristics of these jets in heavy-ion collisions can be compared with the same quantities in pp collisions, where the production of a QGP is not expected. This comparison can provide information about the properties of the QGP and how it interacts with partons from the hard scatter.

Jets with large transverse momenta, p_T^{jet} , in central lead-lead (Pb + Pb) collisions at the LHC are measured at approximately half the rates in pp collisions when the nuclear overlap function of Pb + Pb collisions is taken into account [3–7]. Similarly, back-to-back dijet [8–10] and photon-jet pairs [11,12] are observed to have less-balanced transverse momenta in Pb + Pb collisions compared to pp collisions. These observations suggest that some of the energy from the hard-scattered parton may be transferred outside of the jet through its interaction with the QGP medium.

Complementary measurements look at how the structure of jets in Pb + Pb collisions is modified relative to that in pp collisions. Previous measurements have shown a broadening of jets in Pb + Pb [13–16], as well as an excess of low- and high-momentum charged particles and a depletion of intermediate-momentum charged particles associated with these jets [17–20]. Particles carrying a large fraction of the jet momentum are generally closely aligned with the jet axis, whereas low-momentum particles are observed to have a much broader angular distribution extending outside the jet [9,21–24]. These observations suggest that the energy lost via jet quenching is being transferred to soft particles around the jet axis via soft gluon emission [25–31]. Measurements of yields of these particles as a function of transverse momentum, p_T , and angular distance between the particle and the jet axis have the potential to provide further insight into the structure of jets in the QGP, as well as provide information about how the medium is affected by the presence of the jet.

This paper presents charged-particle p_T distributions at a distance r around the jet axis¹ that have been corrected for

¹ATLAS uses a right-handed coordinate system with its origin at the nominal interaction point (IP) in the center of the detector and the z axis along the beam pipe. The x axis points from the IP to the center of the LHC ring, and the y axis points upward. Cylindrical coordinates (r, ϕ) are used in the transverse plane, with ϕ being the azimuthal angle around the z axis. The pseudorapidity is defined in terms of the polar angle θ as $\eta = -\ln \tan(\theta/2)$. The rapidity is defined as $y = 0.5 \ln[(E + p_z)/(E - p_z)]$ where E and p_z are the energy and z component of the momentum along the

*Full author list given at the end of the article.

Published by the American Physical Society under the terms of the [Creative Commons Attribution 4.0 International](https://creativecommons.org/licenses/by/4.0/) license. Further distribution of this work must maintain attribution to the author(s) and the published article's title, journal citation, and DOI.

detector effects. The measured yields are defined as follows:

$$D(p_T, r) = \frac{1}{N_{\text{jet}}} \frac{1}{2\pi r dr} \frac{dn_{\text{ch}}(p_T, r)}{dp_T},$$

where N_{jet} is the number of jets in consideration and $n_{\text{ch}}(p_T, r)$ is the number of charged particles with a given p_T at a distance r from the jet axis. The ratios of the charged-particle yields measured in Pb + Pb and pp collisions,

$$R_{D(p_T, r)} = \frac{D(p_T, r)_{\text{Pb+Pb}}}{D(p_T, r)_{pp}},$$

quantify the modifications of the yields due to the QGP medium. Furthermore, the differences between the $D(p_T, r)$ distributions in Pb + Pb and pp collisions,

$$\Delta D(p_T, r) = D(p_T, r)_{\text{Pb+Pb}} - D(p_T, r)_{pp},$$

allow the absolute differences in charged-particle yields between the two collision systems to be measured.

II. ATLAS DETECTOR

The measurements presented here are performed using the ATLAS [32] calorimeter, inner detector, trigger, and data-acquisition systems.

The calorimeter system consists of a sampling liquid-argon (LAr) electromagnetic (EM) calorimeter covering $|\eta| < 3.2$, a steel-scintillator sampling hadronic calorimeter covering $|\eta| < 1.7$, LAr hadronic calorimeters covering $1.5 < |\eta| < 3.2$, and two LAr forward calorimeters (FCal) covering $3.1 < |\eta| < 4.9$.

The EM calorimeters are segmented longitudinally in shower depth into three layers with an additional presampler layer. They have segmentation that varies with layer and pseudorapidity. The hadronic calorimeters have three sampling layers longitudinal in shower depth.

The inner detector measures charged particles within the pseudorapidity interval $|\eta| < 2.5$ using a combination of silicon pixel detectors, silicon microstrip detectors (SCT), and a straw-tube transition radiation tracker (TRT), all immersed in a 2-T axial magnetic field. Each of the three detectors is composed of a barrel and two symmetric endcap sections. The pixel detector is composed of four layers, including the insertable B layer [33,34] added in 2014. The SCT barrel section contains four layers of modules with sensors on both sides, and each endcap consists of nine layers of double-sided modules with radial strips. The TRT contains layers of staggered straws interleaved with the transition radiation material.

The zero-degree calorimeters (ZDCs) are located symmetrically at $z = \pm 140$ m and cover $|\eta| > 8.3$. The ZDCs use tungsten plates as absorbers, and quartz rods are sandwiched between the tungsten plates as the active medium. In Pb + Pb

collisions, the ZDCs primarily measure spectator neutrons. These are neutrons that do not interact hadronically when the incident nuclei collide. A ZDC coincidence trigger is implemented by requiring the pulse height from both ZDCs to be above a threshold that accepts the signal corresponding to the energy deposition from a single neutron.

This analysis uses the same trigger setup used in Ref. [20] and is briefly described below. A two-level trigger system was used to select the Pb + Pb and pp collisions. The first level, L1, is based on custom electronics, while the second level, the high-level trigger (HLT), is based on software [35]. Minimum-bias (MB) events were recorded using a logical OR of two triggers: (1) a total-energy L1 trigger selecting more-central collisions and (2) a ZDC coincidence trigger at L1 and a veto on the total-energy trigger, with the additional requirement of at least one track in the HLT, selecting peripheral collisions. The total-energy trigger required the total transverse energy measured in the calorimeter system to be greater than 50 GeV. Jet events were selected by the HLT, seeded by a jet identified by the L1 jet trigger in pp collisions or by the total-energy trigger with a threshold of 50 GeV in Pb + Pb collisions. The L1 jet trigger utilized in pp collisions required a jet with transverse momentum greater than 20 GeV. The HLT jet trigger uses a jet reconstruction procedure similar to that in the offline analysis as discussed in Sec. IV. It selected events containing jets with a transverse energy of at least 75 GeV in Pb + Pb collisions and at least 85 GeV in pp collisions. The measurement is performed in the jet transverse momentum range where the trigger efficiencies are greater than 99%.

III. DATA SETS AND EVENT SELECTION

The Pb + Pb and pp data used in this analysis were recorded in 2015. The data samples consist of 25 pb^{-1} of $\sqrt{s} = 5.02$ TeV pp and 0.49 nb^{-1} of $\sqrt{s_{NN}} = 5.02$ TeV Pb + Pb data. In both samples, events are required to have a reconstructed vertex within 150 mm of the nominal IP along the beam axis. Events with multiple interactions in the same bunch crossing are referred to as pileup. This is negligible in the Pb + Pb data, and the pp data was collected in low-pileup mode. The average number of interactions per bunch crossing in the pp collisions ranged from 0.6 to 1.3. Only events taken during stable beam conditions and satisfying detector and data-quality requirements that include the detector subsystems being in normal operating condition are considered.

In Pb + Pb collisions, the event centrality reflects the overlap area of the two colliding nuclei and is characterized by ΣE_T^{FCal} , the total transverse energy deposited in the FCal [36]. The six centrality intervals used in this analysis are defined according to successive percentiles of the ΣE_T^{FCal} distribution obtained in MB collisions, ordered from the most-central (highest ΣE_T^{FCal}) to the most-peripheral (lowest ΣE_T^{FCal}) collisions: 0–10%, 10–20%, 20–30%, 30–40%, 40–60%, and 60–80%.

The pp Monte Carlo (MC) sample consists of 1.8×10^7 5.02-TeV hard-scattering dijet pp events generated with POWHEG+PYTHIA8 [37–41] using the A14 tune of parameter

beam direction respectively. Transverse momentum and transverse energy are defined as $p_T = p \sin \theta$ and $E_T = E \sin \theta$, respectively. The angular distance between two objects, r , with relative differences $\Delta \eta$ and $\Delta \phi$ in pseudorapidity and azimuth, respectively, is given by $\sqrt{(\Delta \eta)^2 + (\Delta \phi)^2}$.

values [42] and the NNPDF23LO PDF set [43]. The Pb + Pb MC sample was generated by overlaying an additional sample of MB Pb + Pb data events onto a separate set of 1.8×10^7 5.02-TeV hard-scattering dijet pp events generated with the same tune and PDFs as the pp MC sample. This MC overlay sample was reweighted on an event-by-event basis such that it has the same centrality distribution as the jet-triggered data sample. Another sample of MB Pb + Pb events was generated using HIJING (version 1.38b) [44] and was only used to evaluate the track reconstruction performance. The detector response in all MC samples was simulated using GEANT4 [45,46]. These MC samples are used to evaluate the performance of the detector and analysis procedure and correct the measured distributions for detector effects.

IV. JET AND TRACK SELECTION

The jet reconstruction procedure is identical to that used in Ref. [7]. The anti- k_t algorithm [47,48] is first run in four-momentum recombination mode on $\Delta\eta \times \Delta\phi = 0.1 \times 0.1$ calorimeter towers with two anti- k_t radius parameter values ($R = 0.2$ and $R = 0.4$). The energies in the towers are obtained by summing the energies of calorimeter cells at the electromagnetic energy scale. Then, an iterative procedure is used to estimate the η -dependent underlying event (UE) transverse energy density, while excluding the regions populated by jets. The estimate of the UE contribution is performed on an event-by-event basis. Furthermore, the background in Pb + Pb collisions is modulated to account for the azimuthal anisotropy in particle production [49]. The modulation includes the contributions of the second-, third-, and fourth-order azimuthal anisotropy harmonics. The UE transverse energy is subtracted from calorimeter towers included in the jet and the four-momentum of the jet is updated accordingly. Then, a jet η - and p_T -dependent correction factor to the p_T^{jet} derived from the pp MC sample is applied to correct for the calorimeter energy response [50]. The same calibration factors are applied in both the pp and Pb + Pb collisions. An additional correction based on *in situ* studies of jets recoiling against photons, Z bosons, and jets in other regions of the calorimeter is applied [12]. The same jet reconstruction procedure without the azimuthal modulation of the UE is also applied to pp collisions. The UE subtraction in pp collisions removes the pileup contribution to the jet. In this analysis, jets are required to have p_T^{jet} in the 126- to 316-GeV range, with rapidity $|\text{y}^{\text{jet}}| < 1.7$. The p_T^{jet} requirement is chosen in order to exclude the contribution of UE jets generated by fluctuations in the UE, while the rapidity requirement is based on the acceptance of the tracking system. To prevent nearby jets from distorting the measurement of $D(p_T, r)$ distributions, jets are rejected if there is a neighboring jet with higher p_T^{jet} within an angular distance of $\Delta R = 1.0$. This isolation requirement removes approximately 0.01% of jets. Additionally, generator-level jets are reconstructed by applying the anti- k_t algorithm with radius parameter $R = 0.4$ to stable final-state particles from MC generators. These particles are required to have a lifetime of $\tau > 0.3 \times 10^{-10}$ s and do not include muons, neutrinos, and particles from pileup activity.

Charged-particle tracks in Pb + Pb collisions are reconstructed from hits in the inner detector using the track reconstruction algorithm that was optimized for the high hit density in heavy-ion collisions [51]. Tracks used in this analysis have $|\eta| < 2.5$ and are required to have at least 9 (11) total hits in the silicon detectors for charged particles with pseudorapidity $|\eta^{\text{ch}}| \leq 1.65$ ($|\eta^{\text{ch}}| > 1.65$). At least one hit is required in one of the two innermost pixel layers. If the track trajectory passes through an active module in the innermost layer, then a hit in this layer is required. Additionally, a track must have no more than two holes in the pixel and SCT detectors together, where a hole is defined by the absence of a hit predicted by the track trajectory. All charged-particle tracks used in this analysis are required to have reconstructed transverse momentum $p_T^{\text{ch}} > 1.0$ GeV. In order to suppress the contribution from secondary particles,² the distance of closest approach of the track to the primary vertex is required to be less than a value that varies from 0.45 mm at $p_T^{\text{ch}} = 4$ GeV to 0.2 mm at $p_T^{\text{ch}} = 20$ GeV in the transverse plane and less than 1.0 mm in the longitudinal direction. The primary vertex is determined using vertex finding and fitting algorithms described in Ref. [52]. The precision is better than 20 μm in the transverse plane in peripheral collisions and improves inversely proportional to the square root of the number of reconstructed primary tracks in central collisions.

The efficiency, ε , for reconstructing charged particles in Pb + Pb and pp collisions is determined using the MC samples described above. It is evaluated as a function of the generator-level primary particle transverse momentum, p_T^{truth} , and pseudorapidity, η^{truth} , by matching tracks to generator-level primary particles [46]. In both collision systems, the efficiency increases slowly with p_T^{truth} and is seen to be independent of p_T^{jet} in the measurement's phase space. For Pb + Pb collisions, the efficiency for $|\eta| < 0.3$ is $\approx 80\%$ at 1 GeV and rises to $\approx 85\%$ at 10 GeV. For $1.0 < |\eta| < 2.0$, the efficiency is $\approx 67\%$ to $\approx 72\%$ over the same p_T range, with the variation in efficiency between the most-central and most-peripheral Pb + Pb collisions being approximately 3% in both η ranges. For pp collisions, the efficiency for $|\eta| < 0.3$ is $\approx 85\%$ at 1 GeV and rises to $\approx 88\%$ at 10 GeV, remaining relatively constant thereafter. For $1.0 < |\eta| < 2.0$, the efficiency is $\approx 82\%$ to $\approx 86\%$ over the same p_T range. Further details about the tracking efficiency can be found in Ref. [19].

The contribution of reconstructed tracks that cannot be matched to a generated primary particle in the pp MC samples is less than 2% in the entire p_T^{ch} range under study in both the pp and Pb + Pb collisions. This contribution includes fakes and secondaries, where fakes originate from randomly matched hits in the detector layers that do not correspond to the passage of charged particles. Both of these contributions are corrected for as described in the next section.

²Primary particles are defined as particles with a mean lifetime $\tau > 0.3 \times 10^{-10}$ s either directly produced in pp interactions or from subsequent decays of particles with a shorter lifetime. All other particles are considered to be secondary.

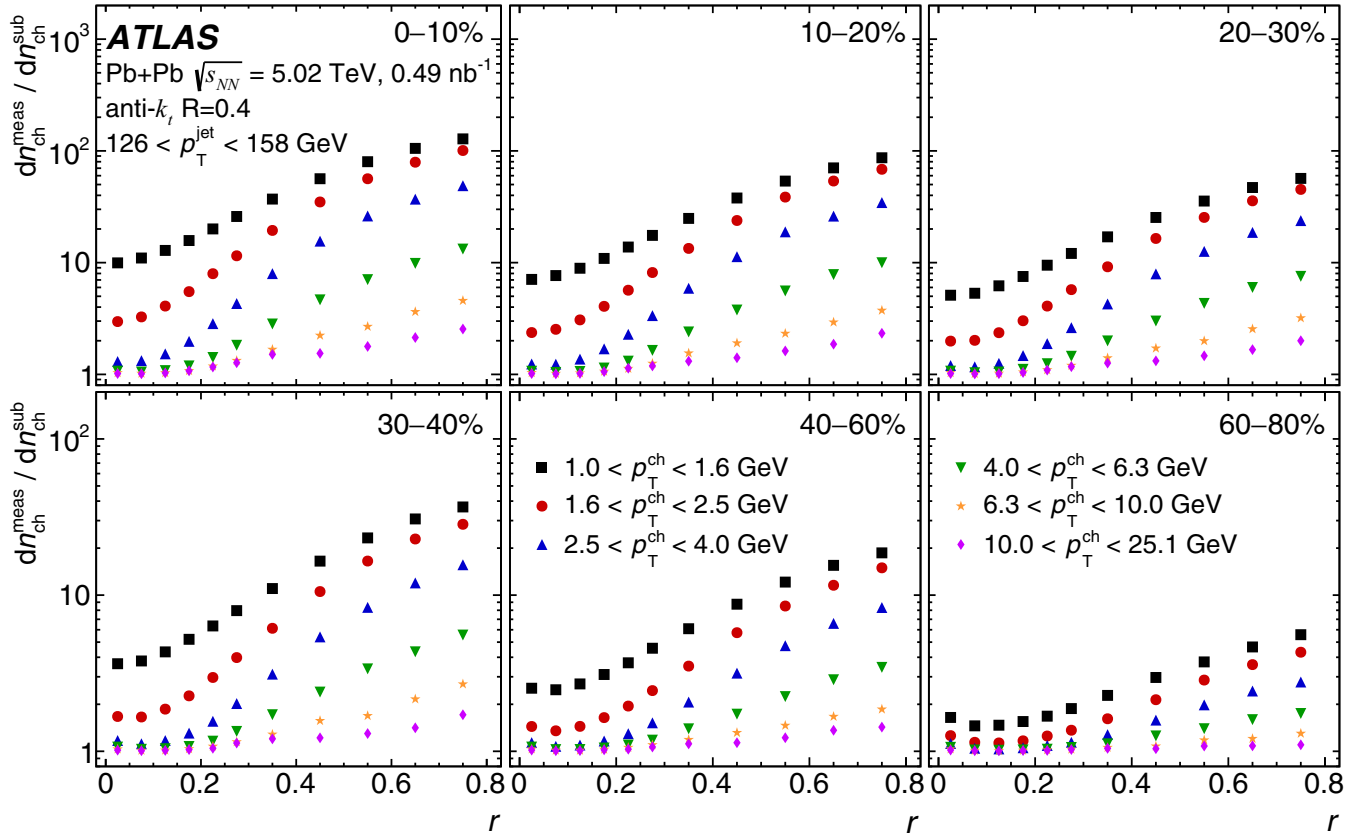


FIG. 1. Ratio of the measured charged-particle distributions to those after the subtraction of the UE, fake tracks, and secondaries as a function of r for different p_T^{ch} intervals for p_T^{jet} in the range 126–158 GeV. The different panels represent the six centrality selections.

V. ANALYSIS PROCEDURE

The analysis procedure is similar to that in Ref. [20], except it is also performed differentially in r . Measured tracks are considered to be associated with a reconstructed jet if their angular distance from the jet axis is less than 0.8. Their multiplicity distribution is given by

$$\frac{d^2 n_{\text{ch}}^{\text{meas}}(p_T^{\text{ch}}, r)}{dp_T^{\text{ch}} dr} = \frac{1}{\varepsilon(p_T^{\text{ch}}, \eta^{\text{ch}})} \frac{\Delta n_{\text{ch}}(p_T^{\text{ch}}, r)}{\Delta p_T^{\text{ch}} \Delta r},$$

where $\Delta n_{\text{ch}}(p_T^{\text{ch}}, r)$ represents the number of tracks within a given Δp_T^{ch} and Δr range. The efficiency correction is applied as a $1/\varepsilon(p_T^{\text{ch}}, \eta^{\text{ch}})$ weight on a track-by-track basis, assuming $p_T^{\text{ch}} = p_T^{\text{truth}}$. While that assumption is not strictly valid, the efficiency varies sufficiently slowly with p_T^{truth} that the error introduced by this assumption is less than 1% and is further corrected for by the Bayesian unfolding procedure described later in this section.

The measured track yields need to be corrected for the contributions from the UE, fake tracks, and secondary particles. In pp collisions, the UE contribution from hard scatterings not associated with jet production is negligible. The contributions from fake tracks and secondary charged particles are estimated from MC samples and subtracted. This procedure is similar to that applied in previous measurements [20,53].

For Pb + Pb collisions, contributions from the UE, fake tracks, and secondary particles are estimated together in a

two-step process: First, the MC overlay sample is used to generate η^{jet} versus ϕ^{jet} maps of the average number of charged particles in a given annulus around a reconstructed jet. This is done for charged particles without an associated generated primary particle and as a function of p_T^{jet} , η^{jet} , ϕ^{jet} , $\Delta\Psi_{\text{jet}}$, r , p_T^{ch} , and centrality. Here $\Delta\Psi_{\text{jet}}$ is the azimuthal angle between the jet and the second-order event plane Ψ_2 and is given by $\Delta\Psi_{\text{jet}} = \phi^{\text{jet}} - \Psi_2$.³ In the second step, the η^{jet} versus ϕ^{jet} maps are used to construct the UE distribution in the data as a function of p_T^{jet} , η^{jet} , ϕ^{jet} , $\Delta\Psi_{\text{jet}}$, and centrality. This distribution includes fakes and tracks from secondary particles and is given by $d^2 n_{\text{ch}}^{\text{UE+Fake}}(p_T^{\text{ch}}, r)/dp_T^{\text{ch}} dr$. The yields decrease with decreasing collision centrality, increasing p_T^{ch} , and increasing $\Delta\Psi_2$. The subtracted distributions are then given by

$$\frac{d^2 n_{\text{ch}}^{\text{sub}}(p_T^{\text{ch}}, r)}{dp_T^{\text{ch}} dr} = \frac{d^2 n_{\text{ch}}^{\text{meas}}(p_T^{\text{ch}}, r)}{dp_T^{\text{ch}} dr} - \frac{d^2 n_{\text{ch}}^{\text{UE+Fake}}(p_T^{\text{ch}}, r)}{dp_T^{\text{ch}} dr}.$$

Figure 1 shows the ratio of the charged-particle distributions before and after the subtraction of the UE, fake tracks, and secondaries, as a function of r for different p_T^{ch} intervals

³The second-order event plane angle Ψ_2 is determined on an event-by-event basis by a standard method using the ϕ variation of transverse energy in the FCal [49].

and $126 < p_T^{\text{jet}} < 158$ GeV for six centrality selections. The largest UE contribution is for 1.0-GeV charged particles at large values of r in central collisions, with the background-to-signal ratio being approximately 100 and slowly decreasing with increasing p_T^{jet} . It rapidly decreases for more-peripheral collisions, larger p_T^{ch} , and smaller r .

To remove the effects of bin migration due to the jet energy and track momentum resolution, the subtracted $d^2n_{\text{ch}}^{\text{sub}}/dp_T^{\text{ch}}dr$ distributions are corrected by a two-dimensional Bayesian unfolding [54] in p_T^{ch} and p_T^{jet} as implemented in the ROOUNFOLD package [55]. Two-dimensional unfolding is used because the calorimetric jet energy response depends on the fragmentation pattern of the jet [56]. Four-dimensional response matrices are created from the pp and Pb + Pb MC samples using the generator-level and reconstructed p_T^{jet} and the generator-level and reconstructed charged-particle p_T^{ch} . They are corrected for tracking efficiencies and are evaluated in bins of r and centrality. The Bayesian procedure requires a choice in the number of iterations. Additional iterations reduce the sensitivity to the choice of prior but may amplify statistical fluctuations in the distributions. After four iterations, the charged-particle distributions are found to be stable within 2–4% for both the Pb + Pb and pp data. A separate one-dimensional Bayesian unfolding is used to correct the measured p_T^{jet} spectra that are used to normalize the unfolded charged-particle distributions. The response matrices for both the one- and two-dimensional unfolding are reweighted such that the $D(p_T, r)$ and p_T^{jet} distributions match the shapes of the corresponding quantities in the reconstructed data.

An independent bin-by-bin unfolding procedure is used to correct for migrations originating from the jet and track angular resolutions. Two corresponding $D(p_T, r)$ distributions are evaluated in MC samples, one using generator-level jets and primary particles, and the other using reconstructed jets and charged particles with their reconstructed p_T replaced by generator-level transverse momentum, p_T^{truth} . The ratio of these two MC distributions provides a correction factor which is then applied to the data. These factors are at the level of approximately 5% with variations up to 15% for particles with $p_T > 4$ GeV, particularly near the edge of the jet. For 126- to 158-GeV jets in Pb + Pb collisions, the full unfolding correction is 8–14% (4–7%) for 1-GeV (6-GeV) tracks, depending on centrality.

The final particle-level corrected distributions, normalized by the area of the annulus being studied, are defined as

$$D(p_T, r) = \frac{1}{N_{\text{jet}}^{\text{unfolded}}} \frac{1}{2\pi r dr} \frac{dn_{\text{ch}}^{\text{unfolded}}(p_T^{\text{ch}}, r)}{dp_T},$$

where $N_{\text{jet}}^{\text{unfolded}}$ is the unfolded number of jets in a given p_T^{jet} interval and $n_{\text{ch}}^{\text{unfolded}}$ is the unfolded yield of charged particles with a given p_T matched to a jet with given p_T^{jet} , at a distance r .

The performance of the full analysis procedure is validated in the MC samples by comparing the fully corrected charged-particle distributions to the generator-level distributions. Good recovery of the generator-level distributions (closure) is observed, with a variation of less than 4% for charged particles

with $p_T < 10$ GeV in both the pp and Pb + Pb collision systems. The nonclosure is taken as an additional systematic uncertainty as discussed in Sec. VI. One important effect is that adding or removing particles carrying a large fraction of the jet momentum near the edge of the jet can significantly alter its reconstructed momentum and direction; this instability contributes to the nonclosure mentioned above for particles with $p_T > 10$ GeV in jets with $p_T^{\text{jet}} < 200$ GeV. Results are presented only where the nonclosure in the pp MC sample is less than 5%.

VI. SYSTEMATIC UNCERTAINTIES

The following sources of systematic uncertainty are considered: the jet energy scale (JES), the jet energy resolution (JER), the sensitivity of the unfolding to the prior, the UE contribution, the residual nonclosure of the analysis procedure, and tracking-related uncertainties. For each variation accounting for a source of systematic uncertainty, the $D(p_T, r)$ distributions along with their ratios and differences are re-evaluated. The difference between the varied and nominal distributions is used as an estimate of the uncertainty.

The systematic uncertainty associated with the JES in Pb + Pb collisions is due to jets having a different structure and possibly a different detector response that is not modeled by the MC simulation. It is composed of two parts: a centrality-independent baseline component and a centrality-dependent component. Only the centrality-independent baseline component is used in pp collisions; it is determined from *in situ* studies of the calorimeter response [50,56,57] and the relative energy scale difference between the jet reconstruction procedures in heavy-ion [57] and pp collisions [50]. The centrality-dependent uncertainty reflects a modification of parton showers by the Pb + Pb environment. It is evaluated by comparing the ratio of the transverse momentum of calorimeter jets to the vectorial sum of the transverse momentum of charged particles within these jet in data and MC events. More details on this procedure can be found in Ref. [7]. The size of the centrality-dependent uncertainty in the JES reaches 0.5% in the most-central collisions. Each component that contributes to the JES uncertainty is varied separately by ± 1 standard deviation for each interval in p_T^{jet} , and the response matrix is recomputed accordingly. The data are then unfolded with the modified matrices. The resulting uncertainty from the JES increases with increasing charged-particle p_T at fixed p_T^{jet} , decreases with increasing p_T^{jet} , and is at the level of 2–4%.

The uncertainty in the $D(p_T, r)$ distributions due to the JER is evaluated by repeating the unfolding procedure with modified response matrices, where an additional contribution is added to the resolution of the reconstructed p_T^{jet} using a Gaussian smearing procedure. The smearing factor is evaluated using an *in situ* technique in 13-TeV pp data that involves studies of dijet energy balance [58,59]. An additional uncertainty is included to account for differences between the tower-based heavy-ion jet reconstruction and that used in analyses of 13-TeV pp data [50,57]. The resulting

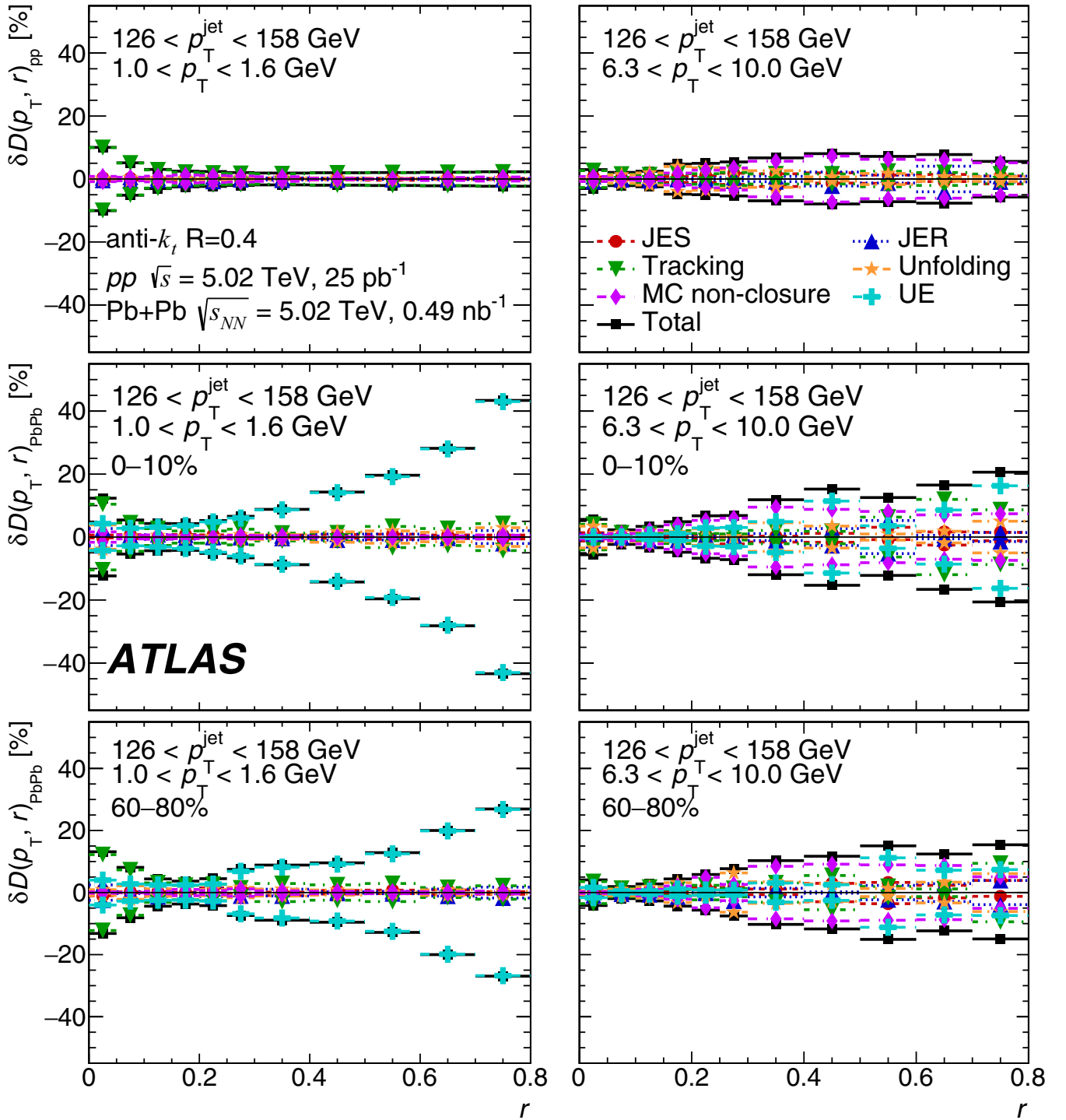


FIG. 2. Relative size of the systematic uncertainties for $D(p_T, r)$ distributions in pp (top), central 0–10% Pb + Pb (middle), and peripheral 60–80% Pb + Pb (bottom) collisions for tracks with $1.0 < p_T < 1.6$ GeV (left) and $6.3 < p_T < 10$ GeV (right) in jets with $126 < p_T^{\text{jet}} < 158$ GeV. The systematic uncertainties due to JES, JER, tracking, unfolding, MC nonclosure, and UE contribution (for Pb + Pb) are shown along with the total systematic uncertainty from all sources.

uncertainty from the JER is symmetrized to account for negative variations of the JER. The size of the resulting uncertainty in the $D(p_T, r)$ distributions due to the JER typically reaches 4–5% for the highest charged-particle p_T intervals and decreases to 2–3% with decreasing charged-particle p_T at fixed p_T^{jet} .

The uncertainties related to track reconstruction and selection originate from several sources. Uncertainties related to the detector material description in simulation and the track transverse momentum resolution are obtained from studies in data and simulation described in Ref. [60]. The sensitivity of the tracking efficiency to the description of the inactive

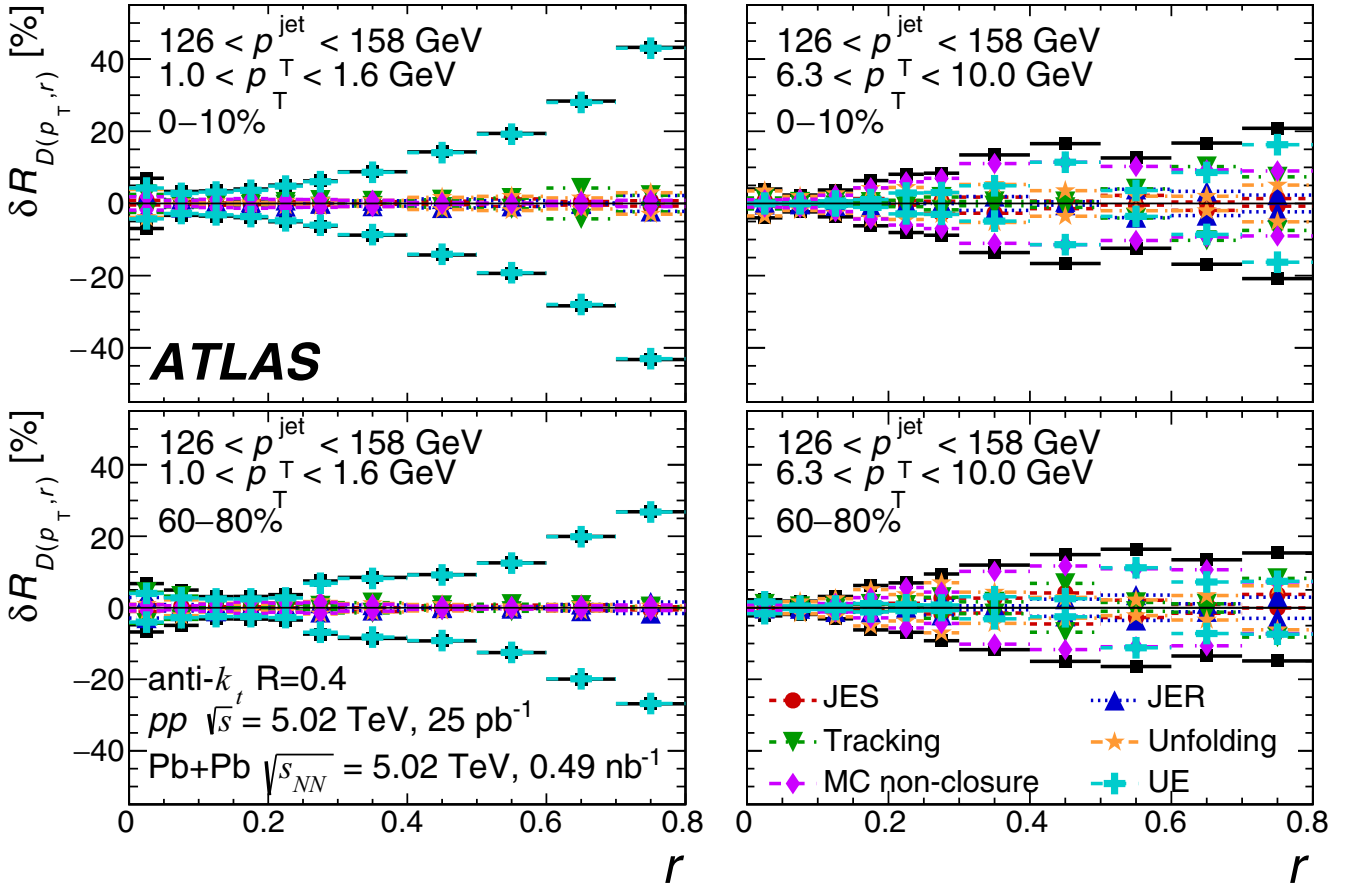


FIG. 3. Relative size of the systematic uncertainties for $R_{D(p_T,r)}$ distributions for 0–10% (top) and 60–80% (bottom) Pb + Pb collisions, for tracks with $1.0 < p_T < 1.6$ GeV (left) and $6.3 < p_T < 10.0$ GeV (right), in jets with $126 < p_T^{\text{jet}} < 158$ GeV. The systematic uncertainties due to JES, JER, tracking, unfolding, MC nonclosure, and UE contribution are shown along with the total systematic uncertainty from all sources.

material in the MC samples is evaluated by varying the material description. This resulting uncertainty in the track reconstruction efficiency is between 0.5% and 2% in the track p_T range used in the analysis. The systematic uncertainty associated with the rate of fakes and secondary tracks is 30% in both collision systems [60]. The contamination of the $n_{\text{ch}}^{\text{sub}}$ from fakes and secondary tracks is approximately 20% in the jet core for tracks with $1 < p_T < 1.6$ GeV. It rapidly decreases as a function of p_T and r and is less than 2% at larger distances from the jet axis. The resulting uncertainty in the $D(p_T, r)$ distributions is at most $\approx 7\%$ in the jet core and decreases as a function of p_T and r . An additional uncertainty takes into account a possible residual misalignment of the tracking detectors in pp and Pb + Pb data collection. The resulting uncertainties in the $D(p_T, r)$ distributions are typically less than 0.1%. An additional uncertainty in the tracking efficiency due to the high local track density in the core of jets is 0.4% [61] for all p_T^{jet} ranges in this analysis. The uncertainty due to the track selection is evaluated by repeating the analysis with an additional 3σ requirement on the significance of the distance of closest approach of the track to the primary vertex. This uncertainty affects the track reconstruction efficiencies, track momentum resolution, and rate of fake tracks. The

resulting uncertainty typically varies between 1% and 2%. Finally, the track-to-particle matching requirements are varied. This variation affects the track reconstruction efficiency, track momentum resolution, and rate of fake tracks. The resulting systematic uncertainty is $\leq 0.1\%$ for the $D(p_T, r)$ distributions. All track-related systematic uncertainties are added in quadrature and presented as the total tracking uncertainty.

The systematic uncertainty associated with the UE subtraction has two components: the limited number of charged particles associated with a jet without a corresponding generator particle in the Pb + Pb MC overlay sample and a comparison with the result of an alternative UE estimation using the cone method. The cone method uses jet-triggered events to estimate the background and is adapted from Refs. [19,20]. A regular grid of nine cones of size $\Delta R = 0.8$ is used to cover the inner-detector region. Cones are excluded if the angular distance to any reconstructed jet in the event with $p_T^{\text{jet}} > 90$ GeV is less than 1.6 or if they contain a charged particle with $p_T > 10$ GeV. This exclusion reduces biases from any hard processes. The resulting UE charged-particle yields $dn_{\text{ch}}^{\text{UE,Cone}}/dp_T^{\text{ch}}$ are evaluated over the 1- to 10-GeV range as a function of p_T^{ch} , p_T^{jet} , centrality, and r , and are

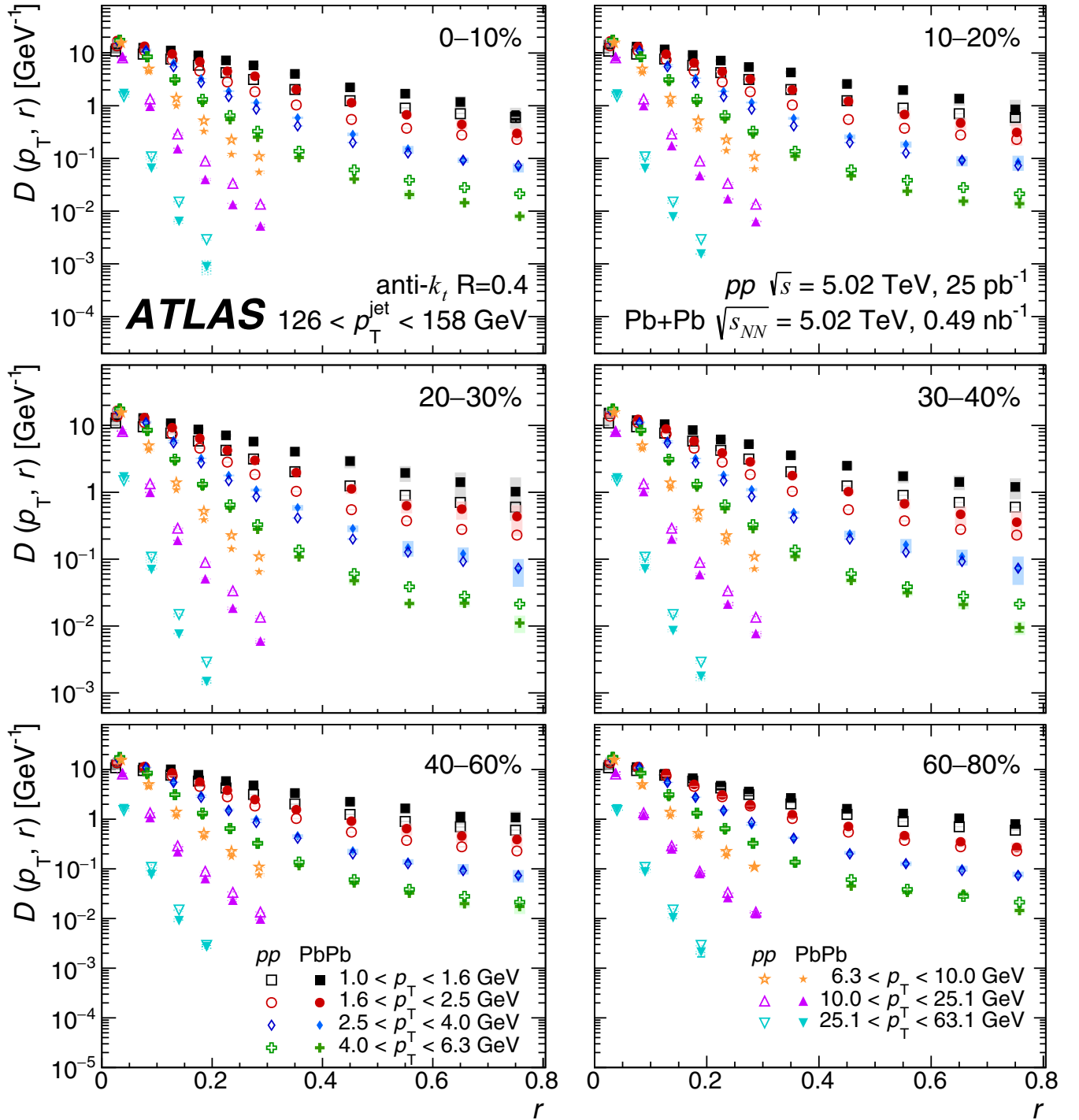


FIG. 4. The $D(p_T, r)$ distributions in pp (open symbols) and $Pb + Pb$ (closed symbols) as a function of angular distance r for p_T^{jet} of 126 to 158 GeV. The symbols represent different track p_T ranges, and each panel is a different centrality selection. The vertical bars on the data points indicate statistical uncertainties, while the shaded boxes indicate systematic uncertainties. The widths of the boxes are not indicative of the bin size, and the points are shifted horizontally for better visibility. The distributions for $p_T > 6.3$ GeV are restricted to smaller r values as discussed in Sec. V.

subsequently averaged over all cones. Both of these sources of uncertainty are combined as uncorrelated uncertainties. The combined UE uncertainty in the $D(p_T, r)$ distributions is less than 10% for $r < 0.4$ and reaches a maximum of 40% at the

largest angular distances from the jet axis. It is the dominant source of systematic uncertainty for low- p_T charged particles at large r and decreases sharply with increasing charged-particle p_T . In particular, the component from the limited

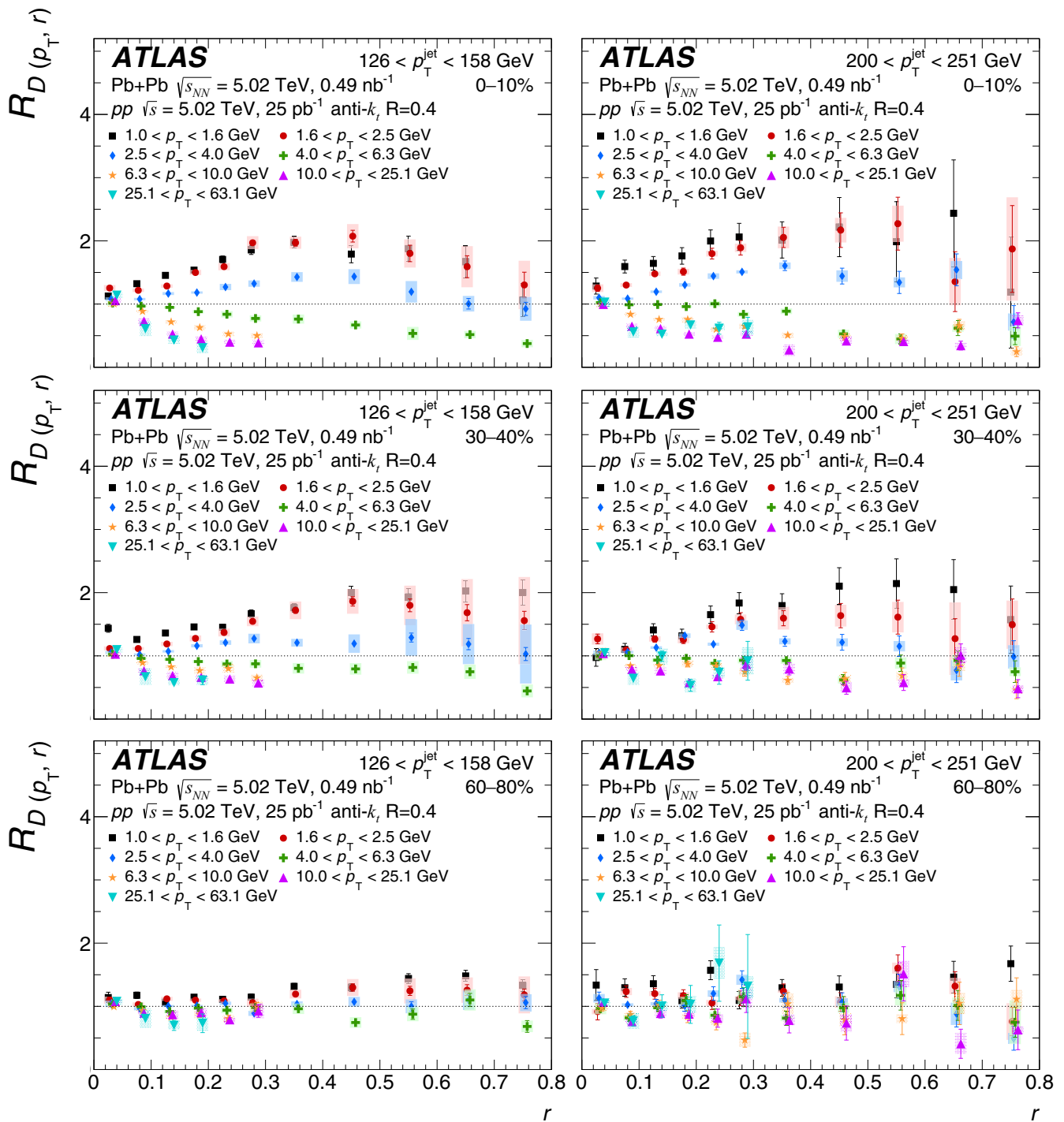


FIG. 5. Ratios of $D(p_T, r)$ distributions in Pb + Pb and pp collisions as a function of angular distance r for $126 < p_T^{\text{jet}} < 158$ GeV (left) and $200 < p_T^{\text{jet}} < 251$ GeV (right) for seven p_T selections. Different centrality selections are shown: 0–10% (top), 30–40% (middle), and 60–80% (bottom). The vertical bars on the data points indicate statistical uncertainties, while the shaded boxes indicate systematic uncertainties. The widths of the boxes are not indicative of the bin size, and the points are shifted horizontally for better visibility.

sample size dominates in the most-central collisions, while the component from the alternative estimation method dominates elsewhere.

The systematic uncertainty in the unfolding procedure is estimated by generating response matrices from the MC distributions without the reweighting that matched the shapes

of the charged-particle and jet distributions in data. The 5–7% difference between the nominal $D(p_T, r)$ distribution and that unfolded with the unweighted response matrix is taken as the systematic uncertainty.

An additional uncertainty to account for possible residual limitations in the analysis procedure is assigned by evaluating

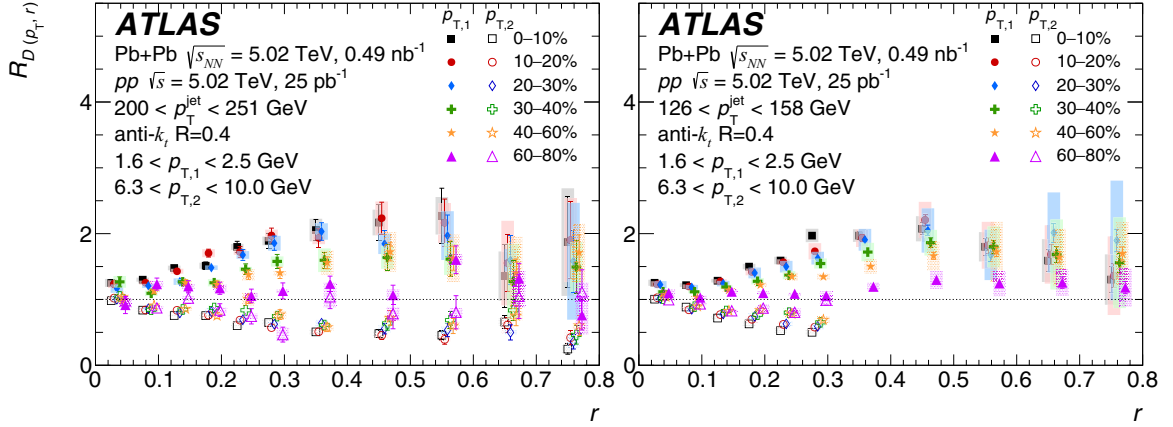


FIG. 6. The $R_{D(p_T, r)}$ distributions for p_T^{jet} of 126–158 GeV (left) and 200–251 GeV (right) as a function of angular distance r for two p_T selections, 1.6–2.5 GeV (closed symbols) and 6.3–10.0 GeV (open symbols), and six centrality intervals. The vertical bars on the data points indicate statistical uncertainties, while the shaded boxes indicate systematic uncertainties. The widths of the boxes are not indicative of the bin size, and the points are shifted horizontally for better visibility.

the nonclosure of the unfolded distributions in simulations. This is typically about 4%.

The correlations between the various systematic components are considered in evaluating the $R_{D(p_T, r)}$ and $\Delta D(p_T, r)$ distributions. The unfolding and nonclosure uncertainties are taken to be uncorrelated between pp and Pb + Pb collisions, while all others are taken to be correlated. For these, the $R_{D(p_T, r)}$ and $\Delta D(p_T, r)$ distributions are re-evaluated by applying the variation to both collision systems; the resulting variations of the ratios from their central values are used as the correlated systematic uncertainty.

Examples of systematic uncertainties in the $D(p_T, r)$ distributions for jets in the 126- to 158-GeV p_T^{jet} range measured in pp and Pb + Pb collision systems are shown in Fig. 2. The uncertainties in the $R_{D(p_T, r)}$ distributions are shown in Fig. 3. It can be seen that the dominant systematic uncertainty in the Pb + Pb and the $R_{D(p_T, r)}$ distributions is from the UE subtraction. While it is less than 5% for $r < 0.3$, it is approximately 40% for charged particles with $p_T = 1$ GeV at $r = 0.8$. The uncertainties in the pp system are smaller, with the dominant systematic uncertainty at low p_T due to the tracking. This is approximately 10% for $r < 0.1$ and decreases to less than 5% at larger distances.

VII. RESULTS

The $D(p_T, r)$ distributions are studied as a function of p_T^{jet} for pp data and Pb + Pb collisions with different centralities. The interplay between the hot and dense matter and the parton shower is explored by evaluating the ratios and differences between the $D(p_T, r)$ distributions in Pb + Pb and pp collisions. Some selected moments of these distributions are also investigated.

A. $D(p_T, r)$ distributions

The $D(p_T, r)$ distributions evaluated in pp and Pb + Pb collisions for $126 < p_T^{\text{jet}} < 158$ GeV are shown in Fig. 4. These distributions decrease as a function of distance from

the jet axis. The rate of fall-off increases sharply for higher p_T particles, with most of these being concentrated near the jet axis. The distributions exhibit a difference in shape between Pb + Pb and pp collisions, with the Pb + Pb distributions being broader at low p_T ($p_T < 4$ GeV) and narrower at high p_T ($p_T > 4$ GeV) in 0–10% central collisions. This modification is centrality dependent and is smaller for peripheral Pb + Pb collisions.

B. $R_{D(p_T, r)}$ distributions

In order to quantify the differences seen in Fig. 4, ratios of the $D(p_T, r)$ distributions in Pb + Pb collisions to those measured in pp collisions for $126 < p_T^{\text{jet}} < 158$ GeV and $200 < p_T^{\text{jet}} < 251$ GeV jets are presented in Fig. 5. They are shown as a function of r for different p_T and centrality selections. In 0–10% central collisions, $R_{D(p_T, r)}$ is greater than unity for $r < 0.8$ for charged particles with p_T less than 4.0 GeV for both p_T^{jet} selections. For these particles, the enhancement of yields in Pb + Pb collisions compared to those in pp collisions grows with increasing r up to approximately $r = 0.3$, with $R_{D(p_T, r)}$ reaching values up to two for $1.0 < p_T < 2.5$ GeV. The value of $R_{D(p_T, r)}$ is approximately constant for r in the interval 0.3–0.6 and decreases for $r > 0.6$. For charged particles with $p_T > 4.0$ GeV, $R_{D(p_T, r)}$ shows a depletion outside the jet core for $r > 0.05$. The magnitude of this depletion increases with increasing r up to $r = 0.3$ and is approximately constant thereafter. For 30–40% midcentral collisions, the enhancement in the yield of particles with $p_T < 4.0$ GeV has trends similar to those in the most central collisions, but the depletion of particles with $p_T > 4.0$ GeV is not as strong. For 60–80% peripheral collisions, $R_{D(p_T, r)}$ has no significant r dependence and the values of $R_{D(p_T, r)}$ are within approximately 50% of unity.

The observed behavior inside the jet cone, $r < 0.4$, agrees with the measurement of the inclusive jet fragmentation functions [10,19,20], where yields of fragments with $p_T < 4$ GeV are observed to be enhanced and yields of charged particles

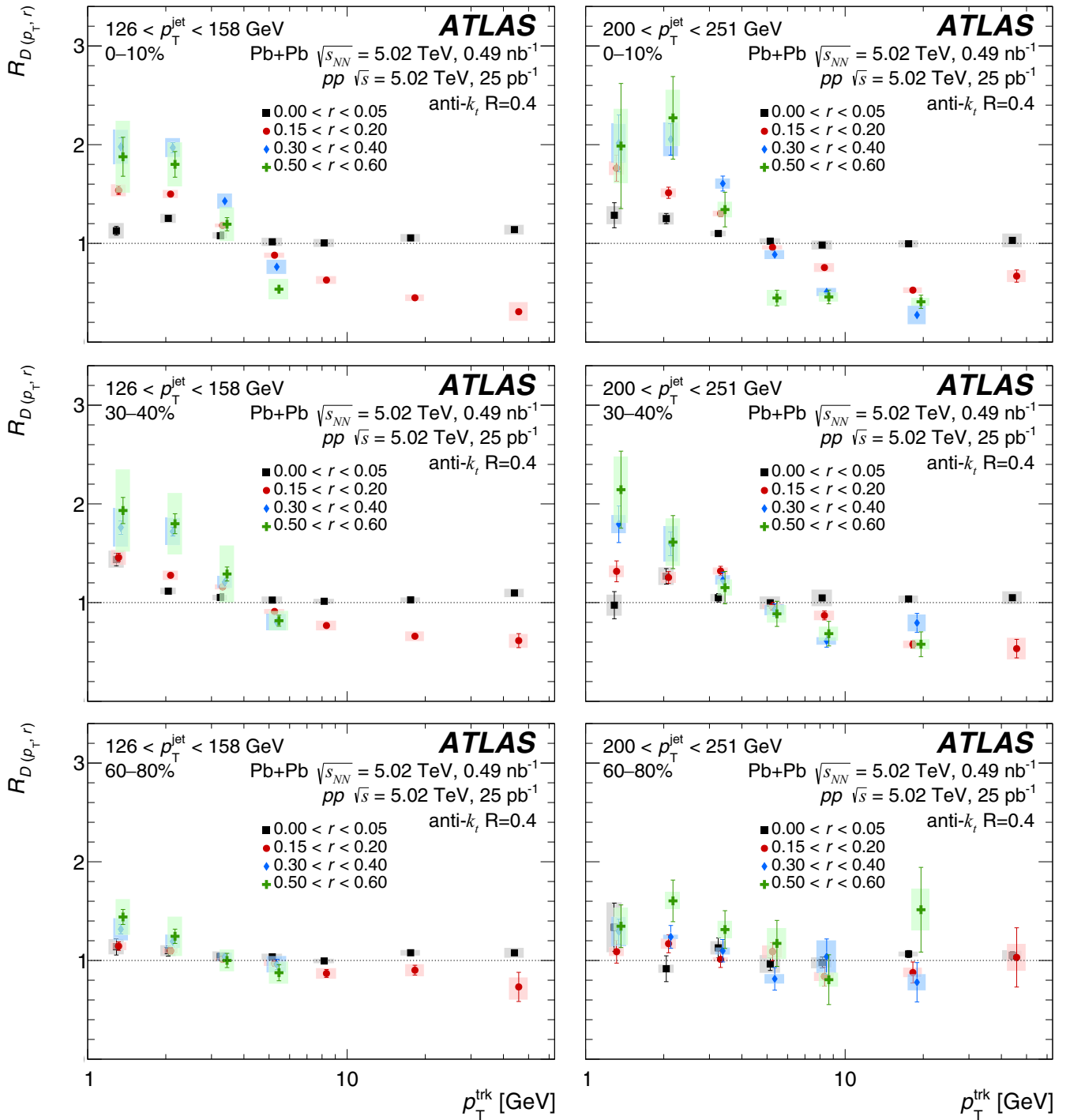


FIG. 7. $R_{D(p_T, r)}$ as a function of p_T for 0–10% (top), 30–40% (middle), and 60–80% (bottom) Pb + Pb collisions in two different p_T^{jet} selections: 126–158 GeV (left) and 200–251 GeV (right). The different colors indicate different angular distances from the jet axis. The vertical bars on the data points indicate statistical uncertainties, while the shaded boxes indicate systematic uncertainties. The widths of the boxes are not indicative of the bin size, and the points are shifted horizontally for better visibility.

with intermediate p_T are suppressed in Pb + Pb collisions compared to those in pp collisions. The wake left in the medium from the passage of the jet compensates for some of the energy it loses [30,31]. The plateau and slight decrease seen in Fig. 5 for the $R_{D(p_T, r)}$ distributions in central Pb + Pb collisions beyond $r = 0.6$ from the jet axis suggests that this

response of the medium is smaller than that predicted in Ref. [31].

The centrality dependence of $R_{D(p_T, r)}$ for two charged-particle p_T intervals (1.6–2.5 GeV and 6.3–10.0 GeV) and two different p_T^{jet} ranges (126–158 GeV and 200–251 GeV) is presented in Fig. 6. For both p_T^{jet} selections, the magnitude

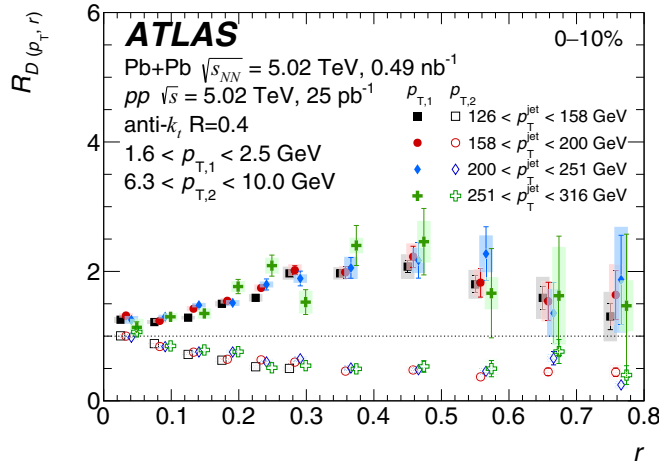


FIG. 8. $R_{D(p_T, r)}$ as a function of r for 0–10% central collisions for charged particles with $1.6 < p_T < 2.5$ GeV (closed symbols) and $6.3 < p_T < 10.0$ GeV (open symbols) for different p_T^{jet} selections. The vertical bars on the data points indicate statistical uncertainties, while the shaded boxes indicate systematic uncertainties. The widths of the boxes are not indicative of the bin size, and the points are shifted horizontally for better visibility.

of the excess for 1.6–2.5 GeV charged particles increases for more-central events and for $r < 0.3$. The magnitude of the excess is approximately a factor of 2 in the most-central collisions for $r > 0.3$. A continuous centrality-dependent suppression of yields of charged particles with $6.3 < p_T < 10.0$ GeV is observed. The magnitude of the modification decreases for more-peripheral collisions in both p_T intervals and p_T^{jet} selections.

Figure 7 shows the charged-particle p_T dependence of $R_{D(p_T, r)}$ for selections in r for jets at 126–158 GeV and 200–251 GeV in the following centrality intervals: 0–10%, 30–40%, and 60–80%. Interestingly, there is no significant suppression of the yields in Pb + Pb collisions for $r < 0.05$ at all measured p_T . For larger r values, the yields are enhanced for charged particles with $p_T < 4$ GeV and suppressed for higher- p_T charged particles in both the 0–10% and 30–40% centrality selections and both p_T^{jet} ranges presented here. The magnitude of the enhancement increases for decreasing p_T below 4 GeV while the suppression is enhanced with increasing p_T for 4–10 GeV, after which it is approximately constant. At fixed p_T the magnitude of the deviation from unity increases for larger distances from the jet axis. In the

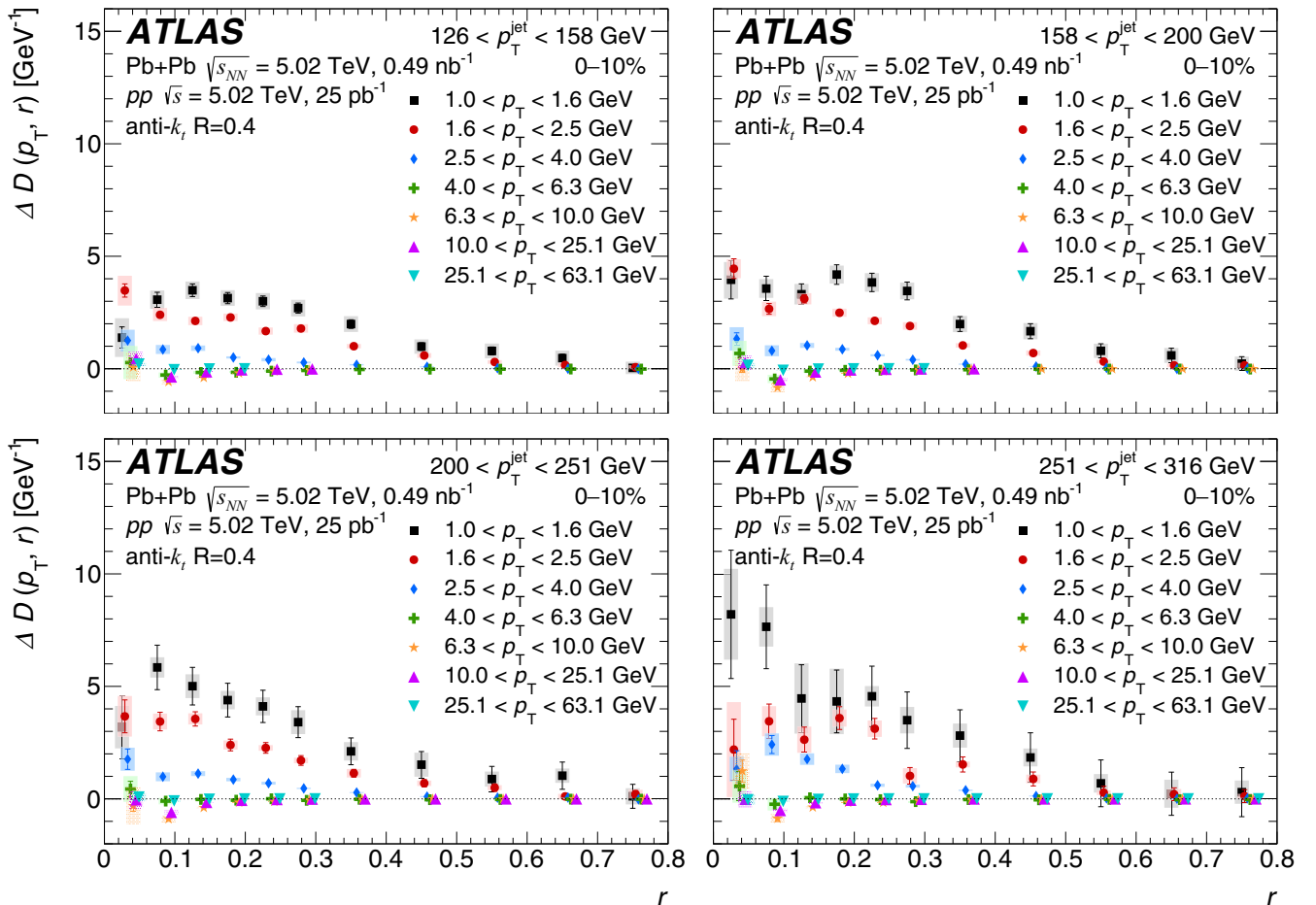


FIG. 9. $\Delta D(p_T, r)$ as a function of r in central collisions for all p_T ranges in four p_T^{jet} selections: 126–158, 158–200, 200–251, and 251–316 GeV. The vertical bars on the data points indicate statistical uncertainties, while the shaded boxes indicate systematic uncertainties. The widths of the boxes are not indicative of the bin size, and the points are shifted horizontally for better visibility.

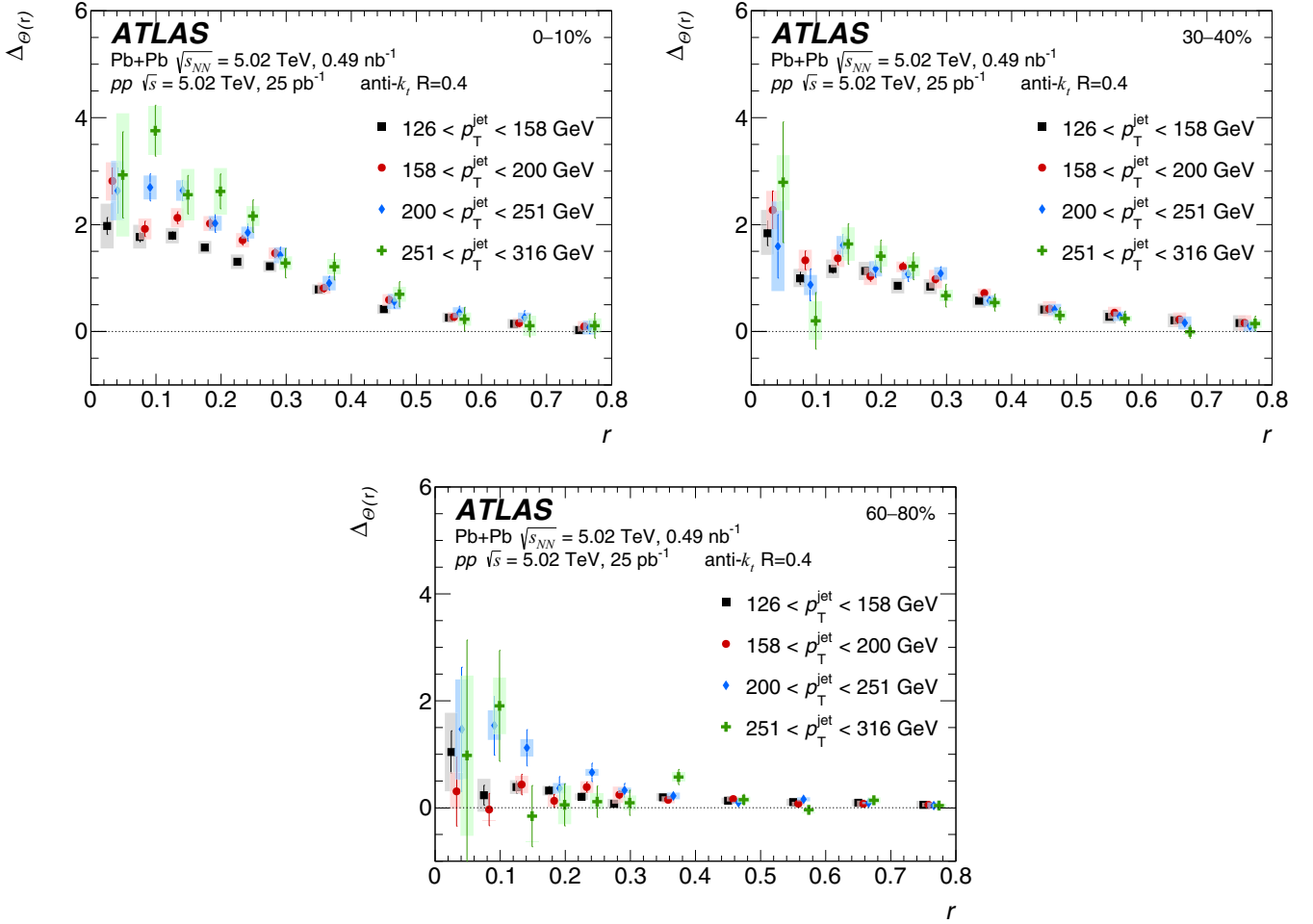


FIG. 10. $\Delta\Theta(r)$ as a function of r for charged particles with $p_T < 4$ GeV in four p_T^{jet} selections, 126–158, 158–200, 200–251, and 251–316 GeV, and three centrality selections, 0–10% (top left), 30–40% (top right), and 60–80% (bottom). The vertical bars on the data points indicate statistical uncertainties, while the shaded boxes indicate systematic uncertainties. The widths of the boxes are not indicative of the bin size, and the points are shifted horizontally for better visibility.

60–80% peripheral collisions, the same trend is seen (but with smaller-magnitude modifications) for $126 < p_T^{\text{jet}} < 158$ GeV; for the higher- p_T^{jet} selection, the larger uncertainties do not allow a clear conclusion to be drawn for peripheral collisions.

The enhancement of the charged-particle yield in the kinematic region of $p_T < 4$ GeV has two possible explanations. First, gluon radiation from the hard-scattered parton as it propagates through the QGP would lead to extra soft particles [62,63]. Second, the interactions of a jet with the QGP and its hydrodynamic response could induce a wake that manifests itself as an enhancement in the number of low- p_T particles [31].

The observed modification at $p_T > 4$ GeV can be explained on the basis of the larger expected energy loss of gluon-initiated jets, resulting in a relative enhancement in the number of quark jets in Pb + Pb collisions compared to pp collisions at a given p_T^{jet} value [20,64]. Since gluon jets have a broader distribution of particle momentum transverse to the jet direction compared to quark-initiated jets [65], the enhanced quark-jet contribution could describe the narrowing of the

particle distribution around the jet direction for particles with $p_T > 4.0$ GeV observed here.

The $R_{D(p_T,r)}$ distributions for low- and high- p_T particles in the different p_T^{jet} selections are directly overlaid in Fig. 8. These distributions are for the 0–10% most-central collisions and show a hint of enhancement in $R_{D(p_T,r)}$ with increasing p_T^{jet} for $r < 0.25$ for low- p_T charged particles. No significant p_T^{jet} dependence is seen at larger r values or for high- p_T charged particles at any r . This p_T^{jet} dependence is further explored by defining an integral over the low- p_T excess and is discussed in Sec. VII D.

C. $\Delta D(p_T, r)$ distributions

In addition to the ratios of the $D(p_T, r)$ distributions, differences between the unfolded charged-particle yields are also evaluated as $\Delta D(p_T, r)$ to quantify the modification in terms of the particle density.

These differences are presented as a function of r for different p_T selections in 0–10% central collisions in Fig. 9. These distributions show an excess in the charged-particle

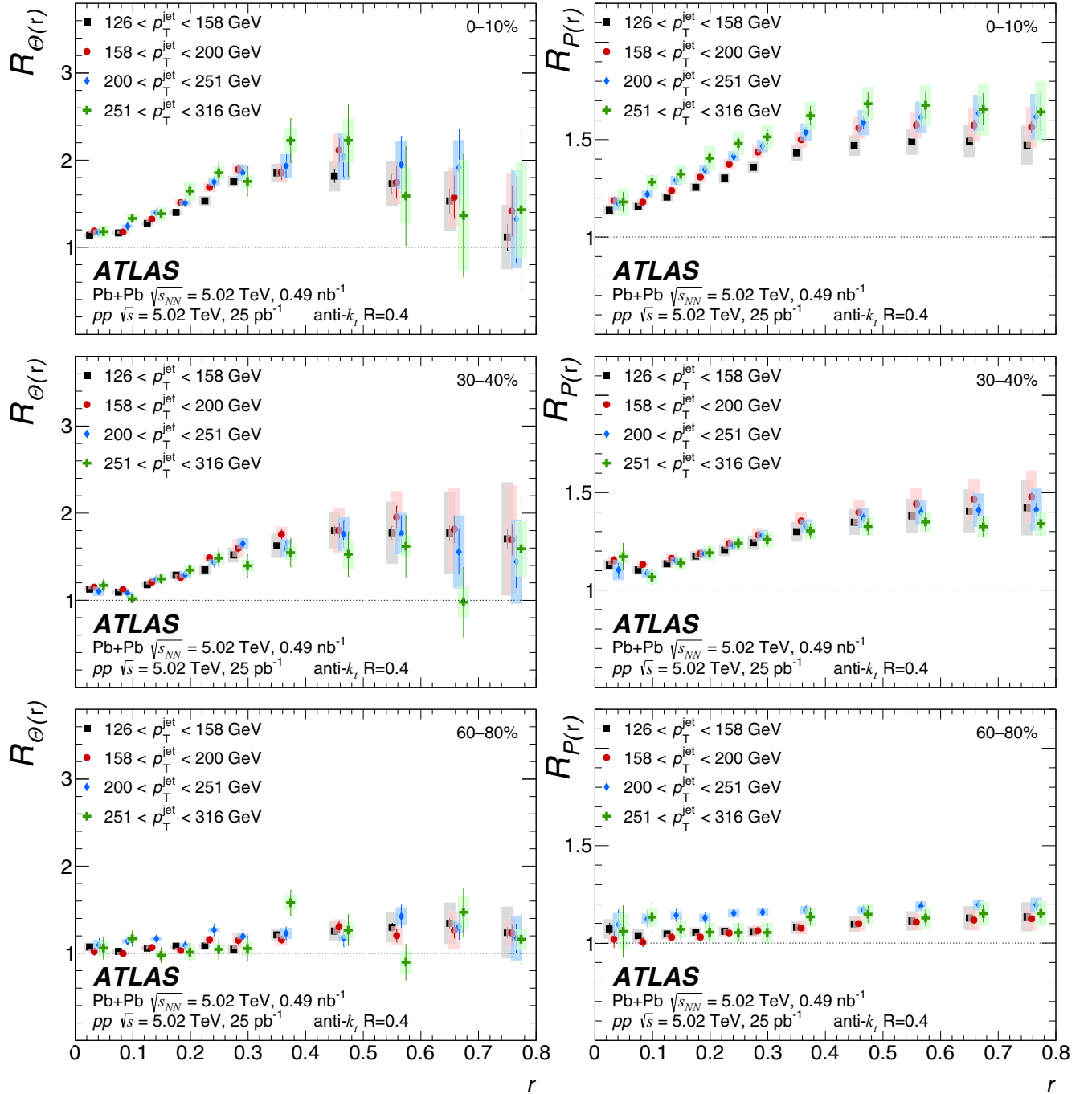


FIG. 11. $R_{\Theta(r)}$ (left) and $R_{P(r)}$ (right) as a function of r for charged particles with $p_T < 4$ GeV ranges in four p_T^{jet} selections, 126–158, 158–200, 200–251, and 251–316 GeV, and three centrality selections, 0–10% (top), 30–40% (middle), and 60–80% (bottom). The vertical bars on the data points indicate statistical uncertainties, while the shaded boxes indicate systematic uncertainties. The widths of the boxes are not indicative of the bin size, and the points are shifted horizontally for better visibility.

yield density for Pb + Pb collisions compared to pp collisions for charged particles with $p_T < 4.0$ GeV. This ranges from 0.5 to 4 particles per unit area per GeV for charged particles with $1 < p_T < 1.6$ GeV in jets with $126 < p_T^{\text{jet}} < 158$ GeV for 0–10% central Pb + Pb collisions and increases with increasing p_T^{jet} . The largest excess for charged particles with $p_T < 4.0$ GeV is within the jet cone. For large r values, the difference decreases but remains positive. A depletion for

higher- p_T particles of up to approximately 0.5 particles per unit area per GeV is seen for 126- to 158-GeV jets in 0–10% central Pb + Pb collisions. The magnitude of this depletion increases for higher p_T^{jet} . A minimum in the $\Delta D(p_T, r)$ distributions for charged particles with $4.0 < p_T < 25.1$ GeV at $0.05 < r < 0.10$ is observed. The magnitudes of the excesses and deficits discussed here depend on the selected charged-particle p_T .

D. p_T integrated distributions

Motivated by similar studies of the enhancement of soft fragments in jet fragmentation functions in Pb + Pb compared to pp collisions from Ref. [20], the unfolded $D(p_T, r)$ distributions are integrated for charged particles with $p_T < 4$ GeV to construct the quantities $\Theta(r)$ and $P(r)$ defined as

$$\Theta(r) = \int_{1 \text{ GeV}}^{4 \text{ GeV}} D(p_T, r) dp_T,$$

$$P(r) = \int_0^r \int_{1 \text{ GeV}}^{4 \text{ GeV}} D(p_T, r') dp_T dr'.$$

The $\Theta(r)$ values are integrated over the charged-particle p_T interval of 1–4 GeV to provide a concise look at the p_T region of enhancement discussed above. The $P(r)$ values further add a running integral over r and provide information about the jet shape. Both of these quantities are compared between the pp and Pb + Pb systems to give the following distributions:

$$\Delta_{\Theta(r)} = \Theta(r)_{\text{Pb+Pb}} - \Theta(r)_{pp},$$

$$R_{\Theta(r)} = \frac{\Theta(r)_{\text{Pb+Pb}}}{\Theta(r)_{pp}},$$

$$R_{P(r)} = \frac{P(r)_{\text{Pb+Pb}}}{P(r)_{pp}}.$$

These integrated quantities are intended to provide aggregate information about the variation with angular distance from the jet axis, magnitude, and p_T^{jet} dependence of the low- p_T charged-particle excess discussed above. The ratio quantities are useful for comparisons with other Pb + Pb measurements $\Delta_{\Theta(r)}$ is comparable to $\Delta D(p_T, r)$, but it is integrated over charged-particle p_T in the 1- to 4-GeV interval [20].

Figure 10 shows the $\Delta_{\Theta(r)}$ distributions as a function of r for the following centrality intervals: 0–10%, 30–40%, and 60–80%. In the most-central collisions, a significant p_T^{jet} dependence of $\Delta_{\Theta(r)}$ is observed; for $r < 0.4$ (particles within the jet cone) $\Delta_{\Theta(r)}$ increases with increasing p_T^{jet} . The value of $\Delta_{\Theta(r)}$ decreases in more-peripheral collisions, where its p_T^{jet} dependence is also no longer significant.

Figure 11 shows the $R_{\Theta(r)}$ and $R_{P(r)}$ distributions as a function of r for the 0–10%, 30–40%, and 60–80% centrality intervals. The $R_{\Theta(r)}$ distributions in the most-central collisions show a maximum for $r \sim 0.4$ and a flattening or a decrease for larger r . However, since $R_{\Theta(r)}$ remains at or above unity for the full range of r values presented, $R_{P(r)}$ shows no suppression with increasing r over the entire measured range. A significant p_T^{jet} dependence is seen in the $R_{P(r)}$ distributions for the most-central Pb + Pb collisions. A slow increase in $R_{P(r)}$ is clearly observed in 30–40% central collisions. In more-peripheral collisions, the magnitude of the excess is reduced and the trends in $R_{\Theta(r)}$ are less clear, although $R_{P(r)}$ is still seen to be above unity. The flattening of the $R_{P(r)}$ distributions at large distances suggests that while wider jets have a softer fragmentation and contain more particles with less p_T in Pb + Pb collisions than in pp collisions [66,67], this effect plateaus for jets with radius larger than 0.6.

VIII. SUMMARY

This paper presents a measurement of the yields of charged particles, $D(p_T, r)$, inside and around $R = 0.4$ anti- k_r jets with $|\eta^{\text{jet}}| < 1.7$ up to an angular distance of $r = 0.8$ from the jet axis, using the ATLAS detector at the LHC. The yields are measured in intervals of p_T^{jet} from 126 to 316 GeV in Pb + Pb and pp collisions at $\sqrt{s_{NN}} = 5.02$ TeV as a function of charged-particle p_T and the angular distance r between the jet axis and charged particle. The integrated luminosities of the Pb + Pb and pp data sets are 0.49 nb^{-1} and 25 pb^{-1} , respectively.

The measurements show a broadening of the $D(p_T, r)$ distribution for low- p_T particles inside the jet in central Pb + Pb collisions compared to those in pp collisions, while for higher- p_T particles the angular distributions are narrower in Pb + Pb collisions than in pp collisions. These modifications are centrality dependent and decrease for more-peripheral collisions. The Pb + Pb-to- pp ratio of the $D(p_T, r)$ distributions, $R_{D(p_T, r)}$, is also examined. The $R_{D(p_T, r)}$ distributions for charged particles with $p_T < 4$ GeV are above unity and grow with increasing angular separation up to $r \sim 0.3$, showing weak to no dependence on r in the interval $0.3 < r < 0.6$ followed with a small decrease in the enhancement for $0.6 < r < 0.8$. For charged particles with $p_T > 4$ GeV, a suppression in $R_{D(p_T, r)}$ is observed and the size of the modification increases with increasing r for $0.05 < r < 0.3$ with no r dependence for $r > 0.3$. For all charged-particle p_T values, the $R_{D(p_T, r)}$ values are greater than or equal to unity for $r < 0.05$. Between $0.1 < r < 0.25$, a statistically significant trend of increasing $R_{D(p_T, r)}$ with increasing p_T^{jet} is observed for low- p_T particles. No significant p_T^{jet} dependence is seen for particles with $p_T > 4$ GeV.

This measurement provides information about the modification of the jet at large distances from the jet axis that can be used to constrain models of how the jet is modified by the presence of the quark-gluon plasma and how the quark-gluon plasma responds to the jet.

ACKNOWLEDGMENTS

We thank CERN for the very successful operation of the LHC. We acknowledge the support of ANPCyT, Argentina; YerPhI, Armenia; ARC, Australia; BMWFW and FWF, Austria; ANAS, Azerbaijan; SSTC, Belarus; CNPq and FAPESP, Brazil; NSERC, NRC and CFI, Canada; CERN; CONICYT, Chile; CAS, MOST, and NSFC, China; COLCIENCIAS, Colombia; MSMT CR, MPO CR, and VSC CR, Czech Republic; DNRF and DNSRC, Denmark; IN2P3-CNRS, CEA-DRF/IRFU, France; SRNSFG, Georgia; BMBF, HGF, and MPG, Germany; GSRT, Greece; RGC, Hong Kong SAR, China; ISF and Benozziyo Center, Israel; INFN, Italy; MEXT and JSPS, Japan; CNRST, Morocco; NWO, Netherlands; RCN, Norway; MNiSW and NCN, Poland; FCT, Portugal; MNE/IFA, Romania; MES of Russia and NRC KI, Russian Federation; JINR; MESTD, Serbia; MSSR, Slovakia; ARRS and MIZŠ, Slovenia; DST/NRF, South Africa; MINECO, Spain; SRC and Wallenberg Foundation, Sweden; SERI, SNSF, and Cantons of Bern and Geneva, Switzerland; MOST,

Taiwan; TAEK, Turkey; STFC, United Kingdom; and DOE and NSF, United States of America. In addition, individual groups and members have received support from BCKDF, CANARIE, CRC, and Compute Canada, Canada; COST, ERC, ERDF, Horizon 2020, and Marie Skłodowska-Curie Actions, European Union; Investissements d' Avenir Labex and Idex, ANR, France; DFG and AvH Foundation, Germany; Herakleitos, Thales, and Aristeia programmes cofinanced by EU-ESF and the Greek NSRF, Greece; BSF-NSF and GIF, Israel; CERCA Programme Generalitat de Catalunya, Spain;

and the Royal Society and Leverhulme Trust, United Kingdom. The crucial computing support from all WLCG partners is acknowledged gratefully, in particular from CERN, the ATLAS Tier-1 facilities at TRIUMF (Canada), NDGF (Denmark, Norway, Sweden), CC-IN2P3 (France), KIT/GridKA (Germany), INFN-CNAF (Italy), NL-T1 (Netherlands), PIC (Spain), ASGC (Taiwan), RAL (UK), and BNL (USA), the Tier-2 facilities worldwide, and large non-WLCG resource providers. Major contributors of computing resources are listed in Ref. [68].

-
- [1] G. Roland, K. Šafařík, and P. Steinberg, Heavy-ion collisions at the LHC, *Prog. Part. Nucl. Phys.* **77**, 70 (2014).
- [2] W. Busza, K. Rajagopal, and W. van der Schee, Heavy ion collisions: The big picture, and the big questions, *Annu. Rev. Nucl. Part. Sci.* **68**, 339 (2018).
- [3] ALICE Collaboration, Measurement of charged jet suppression in Pb-Pb collisions at $\sqrt{s_{NN}} = 2.76$ TeV, *J. High Energy Phys.* **03** (2014) 013.
- [4] ATLAS Collaboration, Measurements of the Nuclear Modification Factor for Jets in Pb + Pb Collisions at $\sqrt{s_{NN}} = 2.76$ TeV with the ATLAS Detector, *Phys. Rev. Lett.* **114**, 072302 (2015).
- [5] ALICE Collaboration, Measurement of jet suppression in central Pb-Pb collisions at $\sqrt{s_{NN}} = 2.76$ TeV, *Phys. Lett. B* **746**, 1 (2015).
- [6] CMS Collaboration, Measurement of inclusive jet cross sections in pp and PbPb collisions at $\sqrt{s_{NN}} = 2.76$ TeV, *Phys. Rev. C* **96**, 015202 (2017).
- [7] ATLAS Collaboration, Measurement of the nuclear modification factor for inclusive jets in Pb + Pb collisions at $\sqrt{s_{NN}} = 5.02$ TeV with the ATLAS detector, *Phys. Lett. B* **790**, 108 (2019).
- [8] ATLAS Collaboration, Observation of a Centrality-Dependent Dijet Asymmetry in Lead-Lead Collisions at $\sqrt{s_{NN}} = 2.76$ TeV with the ATLAS Detector at the LHC, *Phys. Rev. Lett.* **105**, 252303 (2010).
- [9] CMS Collaboration, Observation and studies of jet quenching in PbPb collisions at $\sqrt{s_{NN}} = 2.76$ TeV, *Phys. Rev. C* **84**, 024906 (2011).
- [10] ATLAS Collaboration, Measurement of jet p_T correlations in Pb + Pb and pp collisions at $\sqrt{s_{NN}} = 2.76$ TeV with the ATLAS detector, *Phys. Lett. B* **774**, 379 (2017).
- [11] CMS Collaboration, Studies of jet quenching using isolated-photon+jet correlations in PbPb and pp collisions at $\sqrt{s_{NN}} = 2.76$ TeV, *Phys. Lett. B* **718**, 773 (2013).
- [12] ATLAS Collaboration, Measurement of photon-jet transverse momentum correlations in 5.02 TeV Pb + Pb and pp collisions with ATLAS, *Phys. Lett. B* **789**, 167 (2019).
- [13] ATLAS Collaboration, Measurement of the jet fragmentation function and transverse profile in proton-proton collisions at a center-of-mass energy of 7 TeV with the ATLAS detector, *Eur. Phys. J. C* **71**, 1795 (2011).
- [14] ALICE Collaboration, Medium modification of the shape of small-radius jets in central Pb-Pb collisions at $\sqrt{s_{NN}} = 2.76$ TeV, *J. High Energy Phys.* **10** (2018) 139.
- [15] CMS Collaboration, Shape, transverse size, and charged-hadron multiplicity of jets in pp collisions at $\sqrt{s} = 7$ TeV, *J. High Energy Phys.* **06** (2012) 160.
- [16] CMS Collaboration, Modification of jet shapes in PbPb collisions at $\sqrt{s_{NN}} = 2.76$ TeV, *Phys. Lett. B* **730**, 243 (2014).
- [17] ATLAS Collaboration, Measurement of inclusive jet charged-particle fragmentation functions in Pb + Pb collisions at $\sqrt{s_{NN}} = 2.76$ TeV with the ATLAS detector, *Phys. Lett. B* **739**, 320 (2014).
- [18] CMS Collaboration, Measurement of jet fragmentation in PbPb and pp collisions at $\sqrt{s_{NN}} = 2.76$ TeV, *Phys. Rev. C* **90**, 024908 (2014).
- [19] ATLAS Collaboration, Measurement of jet fragmentation in Pb + Pb and pp collisions at $\sqrt{s_{NN}} = 2.76$ TeV with the ATLAS detector at the LHC, *Eur. Phys. J. C* **77**, 379 (2017).
- [20] ATLAS Collaboration, Measurement of jet fragmentation in Pb + Pb and pp collisions at $\sqrt{s_{NN}} = 5.02$ TeV with the ATLAS detector, *Phys. Rev. C* **98**, 024908 (2018).
- [21] CMS Collaboration, Measurement of transverse momentum relative to dijet systems in PbPb and pp collisions at $\sqrt{s_{NN}} = 2.76$ TeV, *J. High Energy Phys.* **01** (2016) 006.
- [22] CMS Collaboration, Decomposing transverse momentum balance contributions for quenched jets in PbPb collisions at $\sqrt{s_{NN}} = 2.76$ TeV, *J. High Energy Phys.* **11** (2016) 055.
- [23] CMS Collaboration, Jet properties in PbPb and pp collisions at $\sqrt{s_{NN}} = 5.02$ TeV, *J. High Energy Phys.* **05** (2018) 006.
- [24] ALICE Collaboration, Measurement of jet radial profiles in Pb-Pb collisions at $\sqrt{s_{NN}} = 2.76$ TeV, *Phys. Lett. B* **796**, 204 (2019).
- [25] I. Vitev, S. Wicks, and B.-W. Zhang, A theory of jet shapes and cross sections: From hadrons to nuclei, *J. High Energy Phys.* **11** (2008) 093.
- [26] G. Ovanessian and I. Vitev, An effective theory for jet propagation in dense QCD matter: Jet broadening and medium-induced bremsstrahlung, *J. High Energy Phys.* **06** (2011) 080.
- [27] J. P. Blaizot, Y. Mehtar-Tani, and M. A. C. Torres, Angular Structure of the In-Medium QCD Cascade, *Phys. Rev. Lett.* **114**, 222002 (2015).
- [28] G.-Y. Qin and X.-N. Wang, Jet quenching in high-energy heavy-ion collisions, *Int. J. Mod. Phys. E* **24**, 1530014 (2015).
- [29] M. A. Escobedo and E. Iancu, Event-by-event fluctuations in the medium-induced jet evolution, *J. High Energy Phys.* **05** (2016) 008.
- [30] J. Casalderrey-Solana, D. Gulhan, G. Milhano, D. Pablos, and K. Rajagopal, Angular structure of jet quenching within a

- hybrid strong/weak coupling model, *J. High Energy Phys.* **03** (2017) 135.
- [31] Y. Tachibana, N. B. Chang, and G. Y. Qin, Full jet in quark-gluon plasma with hydrodynamic medium response, *Phys. Rev. C* **95**, 044909 (2017).
- [32] ATLAS Collaboration, The ATLAS Experiment at the CERN Large Hadron Collider, *JINST* **3**, S08003 (2008).
- [33] ATLAS Collaboration, ATLAS Insertable B-Layer Technical Design Report, ATLAS-TDR-19, 2010 [<https://cds.cern.ch/record/1291633>]; Addendum: ATLAS-TDR-19-ADD-1, 2012 [<https://cds.cern.ch/record/1451888>]
- [34] B. Abbott, J. Albert, F. Alberti, M. Alex, G. Alimonti, S. Alkire, P. Allport, S. Altenheiner, L. S. Ancu, E. Anderssen *et al.*, Production and integration of the ATLAS Insertable B-Layer, *JINST* **13**, T05008 (2018).
- [35] ATLAS Collaboration, Performance of the ATLAS trigger system in 2015, *Eur. Phys. J. C* **77**, 317 (2017).
- [36] ATLAS Collaboration, Measurement of longitudinal flow decorrelations in Pb + Pb collisions at $\sqrt{s_{NN}} = 2.76$ and 5.02 TeV with the ATLAS detector, *Eur. Phys. J. C* **78**, 142 (2018).
- [37] P. Nason, A new method for combining NLO QCD with shower Monte Carlo algorithms, *J. High Energy Phys.* **11** (2004) 040.
- [38] S. Frixione, P. Nason, and C. Oleari, Matching NLO QCD computations with parton shower simulations: The POWHEG method, *J. High Energy Phys.* **11** (2007) 070.
- [39] S. Alioli, P. Nason, C. Oleari, and E. Re, A general framework for implementing NLO calculations in shower Monte Carlo programs: The POWHEG BOX, *J. High Energy Phys.* **06** (2010) 043.
- [40] S. Alioli, K. Hamilton, P. Nason, C. Oleari, and E. Re, Jet pair production in POWHEG, *J. High Energy Phys.* **04** (2011) 081.
- [41] T. Sjöstrand *et al.*, An introduction to PYTHIA8.2, *Comput. Phys. Commun.* **191**, 159 (2015).
- [42] ATLAS Collaboration, ATLAS PYTHIA8 tunes to 7-TeV data, ATL-PHYS-PUB-2014-021, 2014 [<https://cds.cern.ch/record/1966419>]
- [43] R. D. Ball *et al.*, Parton distributions with LHC data, *Nucl. Phys. B* **867**, 244 (2013).
- [44] X. N. Wang and M. Gyulassy, HIJING: A Monte Carlo model for multiple jet production in pp , pA , and AA collisions, *Phys. Rev. D* **44**, 3501 (1991).
- [45] S. Agostinelli *et al.*, GEANT4: A simulation toolkit, *Nucl. Instrum. Meth. A* **506**, 250 (2003).
- [46] ATLAS Collaboration, The ATLAS simulation infrastructure, *Eur. Phys. J. C* **70**, 823 (2010).
- [47] M. Cacciari, G. P. Salam, and G. Soyez, The anti- k_t jet clustering algorithm, *J. High Energy Phys.* **04** (2008) 063.
- [48] M. Cacciari, G. P. Salam, and G. Soyez, FastJet user manual, *Eur. Phys. J. C* **72**, 1896 (2012).
- [49] ATLAS Collaboration, Measurement of the azimuthal anisotropy for charged particle production in $\sqrt{s_{NN}} = 2.76$ TeV lead-lead collisions with the ATLAS detector, *Phys. Rev. C* **86**, 014907 (2012).
- [50] ATLAS Collaboration, Jet energy scale measurements and their systematic uncertainties in proton-proton collisions at $\sqrt{s} = 13$ TeV with the ATLAS detector, *Phys. Rev. D* **96**, 072002 (2017).
- [51] ATLAS Collaboration, Performance of the ATLAS track reconstruction algorithms in dense environments in LHC run 2, *Eur. Phys. J. C* **77**, 673 (2017).
- [52] ATLAS Collaboration, Performance of primary vertex reconstruction in proton-proton collisions at $\sqrt{s} = 7$ TeV in the ATLAS experiment, ATLAS-CONF-2010-069, 2010 [<https://cds.cern.ch/record/1281344>]
- [53] ATLAS Collaboration, Measurement of jet fragmentation in 5.02 TeV proton-lead and proton-proton collisions with the ATLAS detector, *Nucl. Phys. A* **978**, 65 (2018).
- [54] G. D'Agostini, A multidimensional unfolding method based on Bayes' theorem, *Nucl. Instrum. Meth. A* **362**, 487 (1995).
- [55] T. Auye, Unfolding algorithms and tests using ROOUNFOLD, in *Proceedings of the PHYSTAT 2011 Workshop*, CERN-2011-006 (CERN, Geneva, Switzerland, 2011), pp. 313–318.
- [56] ATLAS Collaboration, Jet energy measurement with the ATLAS detector in proton-proton collisions at $\sqrt{s} = 7$ TeV, *Eur. Phys. J. C* **73**, 2304 (2013).
- [57] ATLAS Collaboration, Jet energy scale and its uncertainty for jets reconstructed using the ATLAS heavy ion jet algorithm, ATLAS-CONF-2015-016, 2015 [<https://cds.cern.ch/record/2008677>]
- [58] ATLAS Collaboration, Jet energy resolution in proton-proton collisions at $\sqrt{s} = 7$ TeV recorded in 2010 with the ATLAS detector, *Eur. Phys. J. C* **73**, 2306 (2013).
- [59] ATLAS Collaboration, Data-driven determination of the energy scale and resolution of jets reconstructed in the ATLAS calorimeters using dijet and multijet events at $\sqrt{s} = 8$ TeV, ATLASCONF-2015-017, 2015 [<https://cds.cern.ch/record/2008678>]
- [60] ATLAS Collaboration, Early inner detector tracking performance in the 2015 data at $\sqrt{s} = 13$ TeV, ATL-PHYS-PUB-2015-051, 2015 [<https://cds.cern.ch/record/2110140>]
- [61] ATLAS Collaboration, Measurement of track reconstruction inefficiencies in the core of jets via pixel dE/dx with the ATLAS experiment using $\sqrt{s} = 13$ TeV pp collision data, ATL-PHYS-PUB-2016-007, 2016 [<https://cds.cern.ch/record/2140460>]
- [62] Y. T. Chien, A. Emerman, Z. B. Kang, G. Ovanessian, and I. Vitev, Jet quenching from QCD evolution, *Phys. Rev. D* **93**, 074030 (2016).
- [63] Z.-B. Kang, F. Ringer, and I. Vitev, Inclusive production of small radius jets in heavy-ion collisions, *Phys. Lett. B* **769**, 242 (2017).
- [64] M. Spousta and B. Cole, Interpreting single jet measurements in Pb + Pb collisions at the LHC, *Eur. Phys. J. C* **76**, 50 (2016).
- [65] OPAL Collaboration, A model independent measurement of quark and gluon jet properties and differences, *Z. Phys. C* **68**, 179 (1995).
- [66] P. M. Chesler and K. Rajagopal, On the evolution of jet energy and opening angle in strongly coupled plasma, *J. High Energy Phys.* **05** (2016) 098.

- [67] Z. Hulcher, D. Pablos, and K. Rajagopal, Resolution effects in the hybrid strong/weak coupling model, *J. High Energy Phys.* **03** (2018) 010.
- [68] ATLAS Collaboration, ATLAS computing acknowledgements, ATL-GEN-PUB-2016-002 [<https://cds.cern.ch/record/2202407>]

G. Aad,¹⁰¹ B. Abbott,¹²⁸ D. C. Abbott,¹⁰² A. Abed Abud,^{70a,70b} K. Abeling,⁵³ D. K. Abhayasinghe,⁹³ S. H. Abidi,¹⁶⁷ O. S. AbouZeid,⁴⁰ N. L. Abraham,¹⁵⁶ H. Abramowicz,¹⁶¹ H. Abreu,¹⁶⁰ Y. Abulaiti,⁶ B. S. Acharya,^{66a,66b,o} B. Achkar,⁵³ S. Adachi,¹⁶³ L. Adam,⁹⁹ C. Adam Bourdarios,⁵ L. Adamczyk,^{83a} L. Adamek,¹⁶⁷ J. Adelman,¹²¹ M. Adersberger,¹¹⁴ A. Adiguzel,^{12c} S. Adorni,⁵⁴ T. Adye,¹⁴⁴ A. A. Affolder,¹⁴⁶ Y. Afik,¹⁶⁰ C. Agapopoulou,¹³² M. N. Agaras,³⁸ A. Aggarwal,¹¹⁹ C. Agheorghiesei,^{27c} J. A. Aguilar-Saavedra,^{140f,140a,ai} F. Ahmadov,⁷⁹ W. S. Ahmed,¹⁰³ X. Ai,¹⁸ G. Aielli,^{73a,73b} S. Akatsuka,⁸⁵ T. P. A. Åkesson,⁹⁶ E. Akilli,⁵⁴ A. V. Akimov,¹¹⁰ K. Al Khoury,¹³² G. L. Alberghi,^{23b,23a} J. Albert,¹⁷⁶ M. J. Alconada Verzini,¹⁶¹ S. Alderweireldt,³⁶ M. Aleksa,³⁶ I. N. Aleksandrov,⁷⁹ C. Alexa,^{27b} D. Alexandre,¹⁹ T. Alexopoulos,¹⁰ A. Alfonsi,¹²⁰ F. Alfonsi,^{23b,23a} M. Alhroob,¹²⁸ B. Ali,¹⁴² G. Alimonti,^{68a} J. Alison,³⁷ S. P. Alkire,¹⁴⁸ C. Allaire,¹³² B. M. M. Allbrooke,¹⁵⁶ B. W. Allen,¹³¹ P. P. Allport,²¹ A. Aloisio,^{69a,69b} A. Alonso,⁴⁰ F. Alonso,⁸⁸ C. Alpigiani,¹⁴⁸ A. A. Alshehri,⁵⁷ M. Alvarez Estevez,⁹⁸ D. Álvarez Piqueras,¹⁷⁴ M. G. Alvisi,^{69a,69b} Y. Amaral Coutinho,^{80b} A. Ambler,¹⁰³ L. Ambroz,¹³⁵ C. Amelung,²⁶ D. Amidei,¹⁰⁵ S. P. Amor Dos Santos,^{140a} S. Amoroso,⁴⁶ C. S. Amrouche,⁵⁴ F. An,⁷⁸ C. Anastopoulos,¹⁴⁹ N. Andari,¹⁴⁵ T. Andeen,¹¹ C. F. Anders,^{61b} J. K. Anders,²⁰ A. Andreazza,^{68a,68b} V. Andrei,^{61a} C. R. Anelli,¹⁷⁶ S. Angelidakis,³⁸ A. Angerami,³⁹ A. V. Anisenkov,^{122b,122a} A. Annovi,^{71a} C. Antel,^{61a} M. T. Anthony,¹⁴⁹ M. Antonelli,⁵¹ D. J. A. Antrim,¹⁷¹ F. Anulli,^{72a} M. Aoki,⁸¹ J. A. Aparisi Pozo,¹⁷⁴ L. Aperio Bella,^{15a} G. Arabidze,¹⁰⁶ J. P. Araque,^{140a} V. Araujo Ferraz,^{80b} R. Araujo Pereira,^{80b} C. Arcangeletti,⁵¹ A. T. H. Arce,⁴⁹ F. A. Arduh,⁸⁸ J.-F. Arguin,¹⁰⁹ S. Argyropoulos,⁷⁷ J.-H. Arling,⁴⁶ A. J. Armbruster,³⁶ A. Armstrong,¹⁷¹ O. Arnaez,¹⁶⁷ H. Arnold,¹²⁰ Z. P. Arrubarrena Tame,¹¹⁴ A. Artamonov,^{111,*} G. Artoni,¹³⁵ S. Artz,⁹⁹ S. Asai,¹⁶³ N. Asbah,⁵⁹ E. M. Asimakopoulou,¹⁷² L. Asquith,¹⁵⁶ J. Assahsah,^{35d} K. Assamagan,²⁹ R. Astalos,^{28a} R. J. Atkin,^{33a} M. Atkinson,¹⁷³ N. B. Atlay,¹⁹ H. Atmani,¹³² K. Augsten,¹⁴² G. Avolio,³⁶ R. Avramidou,^{60a} M. K. Ayoub,^{15a} A. M. Azoulay,^{168b} G. Azuelos,^{109,ax} H. Bachacou,¹⁴⁵ K. Bachas,^{67a,67b} M. Backes,¹³⁵ F. Backman,^{45a,45b} P. Bagnaia,^{72a,72b} M. Bahmani,⁸⁴ H. Bahrasemani,¹⁵² A. J. Bailey,¹⁷⁴ V. R. Bailey,¹⁷³ J. T. Baines,¹⁴⁴ M. Bajic,⁴⁰ C. Bakalis,¹⁰ O. K. Baker,¹⁸³ P. J. Bakker,¹²⁰ D. Bakshi Gupta,⁸ S. Balaji,¹⁵⁷ E. M. Baldin,^{122b,122a} P. Balek,¹⁸⁰ F. Balli,¹⁴⁵ W. K. Balunas,¹³⁵ J. Balz,⁹⁹ E. Banas,⁸⁴ A. Bandyopadhyay,²⁴ Sw. Banerjee,^{181,j} A. A. E. Bannoura,¹⁸² L. Barak,¹⁶¹ W. M. Barbe,³⁸ E. L. Barberio,¹⁰⁴ D. Barberis,^{55b,55a} M. Barbero,¹⁰¹ G. Barbour,⁹⁴ T. Barillari,¹¹⁵ M.-S. Barisits,³⁶ J. Barkeloo,¹³¹ T. Barklow,¹⁵³ R. Barnea,¹³¹ S. L. Barnes,^{60c} B. M. Barnett,¹⁴⁴ R. M. Barnett,¹⁸ Z. Barnovska-Blenessy,^{60a} A. Baroncelli,^{60a} G. Barone,²⁹ A. J. Barr,¹³⁵ L. Barranco Navarro,^{45a,45b} F. Barreiro,⁹⁸ J. Barreiro Guimarães da Costa,^{15a} S. Barsov,¹³⁸ R. Bartoldus,¹⁵³ G. Bartolini,¹⁰¹ A. E. Barton,⁸⁹ P. Bartos,^{28a} A. Basalaeu,⁴⁶ A. Bassalat,^{132,aq} M. J. Basso,¹⁶⁷ R. L. Bates,⁵⁷ S. Batlamous,^{35e} J. R. Batley,³² B. Batool,¹⁵¹ M. Battaglia,¹⁴⁶ M. Bause,^{72a,72b} F. Bauer,¹⁴⁵ K. T. Bauer,¹⁷¹ H. S. Bawa,^{31,m} J. B. Beacham,⁴⁹ T. Beau,¹³⁶ P. H. Beauchemin,¹⁷⁰ F. Becherer,⁵² P. Bechtel,²⁴ H. C. Beck,⁵³ H. P. Beck,^{20,s} K. Becker,⁵² M. Becker,⁹⁹ C. Becot,⁴⁶ A. Beddall,^{12d} A. J. Beddall,^{12a} V. A. Bednyakov,⁷⁹ M. Bedognetti,¹²⁰ C. P. Bee,¹⁵⁵ T. A. Beermann,⁷⁶ M. Begalli,^{80b} M. Begel,²⁹ A. Behera,¹⁵⁵ J. K. Behr,⁴⁶ F. Beisiegel,²⁴ A. S. Bell,⁹⁴ G. Bella,¹⁶¹ L. Bellagamba,^{23b} A. Bellerive,³⁴ P. Bellos,⁹ K. Beloborodov,^{122b,122a} K. Belotskiy,¹¹² N. L. Belyaev,¹¹² D. Benckekroun,^{35a} N. Benekos,¹⁰ Y. Benhammou,¹⁶¹ D. P. Benjamin,⁶ M. Benoit,⁵⁴ J. R. Bensinger,²⁶ S. Bentvelsen,¹²⁰ L. Beresford,¹³⁵ M. Beretta,⁵¹ D. Berge,⁴⁶ E. Bergeaas Kuutmann,¹⁷² N. Berger,⁵ B. Bergmann,¹⁴² L. J. Bergsten,²⁶ J. Beringer,¹⁸ S. Berlendis,⁷ N. R. Bernard,¹⁰² G. Bernardi,¹³⁶ C. Bernius,¹⁵³ T. Berry,⁹³ P. Berta,⁹⁹ C. Bertella,^{15a} I. A. Bertram,⁸⁹ O. Bessidskaia Bylund,¹⁸² N. Besson,¹⁴⁵ A. Bethani,¹⁰⁰ S. Bethke,¹¹⁵ A. Betti,²⁴ A. J. Bevan,⁹² J. Beyer,¹¹⁵ D. S. Bhattacharya,¹⁷⁷ P. Bhattarai,²⁶ R. Bi,¹³⁹ R. M. Bianchi,¹³⁹ O. Biebel,¹¹⁴ D. Biedermann,¹⁹ R. Bielski,³⁶ K. Bierwagen,⁹⁹ N. V. Biesuz,^{71a,71b} M. Biglietti,^{74a} T. R. V. Billoud,¹⁰⁹ M. Bindi,⁵³ A. Bingul,^{12d} C. Bini,^{72a,72b} S. Biondi,^{23b,23a} M. Birman,¹⁸⁰ T. Bisanz,⁵³ J. P. Biswal,¹⁶¹ D. Biswas,^{181,j} A. Bitadze,¹⁰⁰ C. Bittrich,⁴⁸ K. Björke,¹³⁴ K. M. Black,²⁵ T. Blazek,^{28a} I. Bloch,⁴⁶ C. Blocker,²⁶ A. Blue,⁵⁷ U. Blumenschein,⁹² G. J. Bobbink,¹²⁰ V. S. Bobrovnikov,^{122b,122a} S. S. Bocchetta,⁹⁶ A. Bocci,⁴⁹ D. Boerner,⁴⁶ D. Bogavac,¹⁴ A. G. Bogdanchikov,^{122b,122a} C. Bohm,^{45a} V. Boisvert,⁹³ P. Bokan,^{53,172} T. Bold,^{83a} A. S. Boldyrev,¹¹³ A. E. Bolz,^{61b} M. Bomben,¹³⁶ M. Bona,⁹² J. S. Bonilla,¹³¹ M. Boonekamp,¹⁴⁵ C. D. Booth,⁹³ H. M. Borecka-Bielska,⁹⁰ A. Borisov,¹²³ G. Borissov,⁸⁹ J. Bortfeldt,³⁶ D. Bortoletto,¹³⁵ D. Boscherini,^{23b} M. Bosman,¹⁴ J. D. Bossio Sola,¹⁰³ K. Bouaouda,^{35a} J. Boudreau,¹³⁹ E. V. Bouhova-Thacker,⁸⁹ D. Boumediene,³⁸ S. K. Boutle,⁵⁷ A. Boveia,¹²⁶ J. Boyd,³⁶ D. Boye,^{33b,ar} I. R. Boyko,⁷⁹ A. J. Bozson,⁹³ J. Bracinek,²¹ N. Brahimi,¹⁰¹ G. Brandt,¹⁸² O. Brandt,³² F. Braren,⁴⁶ B. Brau,¹⁰² J. E. Brau,¹³¹ W. D. Breaden Madden,⁵⁷ K. Brendlinger,⁴⁶ L. Brenner,⁴⁶ R. Brenner,¹⁷² S. Bressler,¹⁸⁰ B. Brickwedde,⁹⁹ D. L. Briglin,²¹ D. Britton,⁵⁷ D. Britzger,¹¹⁵ I. Brock,²⁴ R. Brock,¹⁰⁶ G. Brooijmans,³⁹ W. K. Brooks,^{147b} E. Brost,¹²¹ J. H. Broughton,²¹ P. A. Bruckman de Renstrom,⁸⁴ D. Bruncko,^{28b} A. Bruni,^{23b} G. Bruni,^{23b} L. S. Bruni,¹²⁰ S. Bruno,^{73a,73b} B. H. Brunt,³² M. Bruschi,^{23b} N. Bruscino,¹³⁹ P. Bryant,³⁷ L. Bryngemark,⁹⁶ T. Buanes,¹⁷ Q. Buat,³⁶ P. Buchholz,¹⁵¹ A. G. Buckley,⁵⁷ I. A. Budagov,⁷⁹ M. K. Bugge,¹³⁴ F. Bühner,⁵² O. Bulekov,¹¹² T. J. Burch,¹²¹ S. Burdin,⁹⁰ C. D. Burgard,¹²⁰ A. M. Burger,¹²⁹ B. Burghgrave,⁸ J. T. P. Burr,⁴⁶ C. D. Burton,¹¹ J. C. Burzynski,¹⁰² V. Büscher,⁹⁹ E. Buschmann,⁵³ P. J. Bussey,⁵⁷ J. M. Butler,²⁵ C. M. Buttar,⁵⁷ J. M. Butterworth,⁹⁴ P. Butti,³⁶ W. Buttinger,³⁶

- C. J. Buxo Vazquez,¹⁰⁶ A. Buzatu,¹⁵⁸ A. R. Buzykaev,^{122b,122a} G. Cabras,^{23b,23a} S. Cabrera Urbán,¹⁷⁴ D. Caforio,⁵⁶ H. Cai,¹⁷³ V. M. M. Cairo,¹⁵³ O. Cakir,^{4a} N. Calace,³⁶ P. Calafiura,¹⁸ A. Calandri,¹⁰¹ G. Calderini,¹³⁶ P. Calfayan,⁶⁵ G. Callea,⁵⁷ L. P. Caloba,^{80b} S. Calvente Lopez,⁹⁸ D. Calvet,³⁸ S. Calvet,³⁸ T. P. Calvet,¹⁵⁵ M. Calvetti,^{71a,71b} R. Camacho Toro,¹³⁶ S. Camarda,³⁶ D. Camarero Munoz,⁹⁸ P. Camarri,^{73a,73b} D. Cameron,¹³⁴ R. Caminal Armadans,¹⁰² C. Camincher,³⁶ S. Campana,³⁶ M. Campanelli,⁹⁴ A. Camplani,⁴⁰ A. Campoverde,¹⁵¹ V. Canale,^{69a,69b} A. Canesse,¹⁰³ M. Cano Bret,^{60c} J. Cantero,¹²⁹ T. Cao,¹⁶¹ Y. Cao,¹⁷³ M. D. M. Capeans Garrido,³⁶ M. Capua,^{41b,41a} R. Cardarelli,^{73a} F. Cardillo,¹⁴⁹ G. Carducci,^{41b,41a} I. Carli,¹⁴³ T. Carli,³⁶ G. Carlino,^{69a} B. T. Carlson,¹³⁹ L. Carminati,^{68a,68b} R. M. D. Carney,^{45a,45b} S. Caron,¹¹⁹ E. Carquin,^{147b} S. Carrá,⁴⁶ J. W. S. Carter,¹⁶⁷ M. P. Casado,^{14,e} A. F. Casha,¹⁶⁷ D. W. Casper,¹⁷¹ R. Castelijns,¹²⁰ F. L. Castillo,¹⁷⁴ V. Castillo Gimenez,¹⁷⁴ N. F. Castro,^{140a,140e} A. Catinaccio,³⁶ J. R. Catmore,¹³⁴ A. Cattai,³⁶ J. Caudron,²⁴ V. Cavaliere,²⁹ E. Cavallaro,¹⁴ M. Cavalli-Sforza,¹⁴ V. Cavasinni,^{71a,71b} E. Celebi,^{12b} F. Ceradini,^{74a,74b} L. Cerda Alberich,¹⁷⁴ K. Cerny,¹³⁰ A. S. Cerqueira,^{80a} A. Cerri,¹⁵⁶ L. Cerrito,^{73a,73b} F. Cerutti,¹⁸ A. Cervelli,^{23b,23a} S. A. Cetin,^{12b} Z. Chadi,^{35a} D. Chakraborty,¹²¹ S. K. Chan,⁵⁹ W. S. Chan,¹²⁰ W. Y. Chan,⁹⁰ J. D. Chapman,³² B. Chargeishvili,^{159b} D. G. Charlton,²¹ T. P. Charman,⁹² C. C. Chau,³⁴ S. Che,¹²⁶ S. Chekanov,⁶ S. V. Chekulaev,^{168a} G. A. Chelkov,^{79,aw} M. A. Chelstowska,³⁶ B. Chen,⁷⁸ C. Chen,^{60a} C. H. Chen,⁷⁸ H. Chen,²⁹ J. Chen,^{60a} J. Chen,³⁹ S. Chen,¹³⁷ S. J. Chen,^{15c} X. Chen,^{15b,av} Y. Chen,⁸² Y-H. Chen,⁴⁶ H. C. Cheng,^{63a} H. J. Cheng,^{15a,15d} A. Cheplakov,⁷⁹ E. Cheremushkina,¹²³ R. Cherkaoui El Moursli,^{35e} E. Cheu,⁷ K. Cheung,⁶⁴ T. J. A. Chevalérias,¹⁴⁵ L. Chevalier,¹⁴⁵ V. Chiarella,⁵¹ G. Chiarelli,^{71a} G. Chiodini,^{67a} A. S. Chisholm,²¹ A. Chitan,^{27b} I. Chiu,¹⁶³ Y. H. Chiu,¹⁷⁶ M. V. Chizhov,⁷⁹ K. Choi,⁶⁵ A. R. Chomont,^{72a,72b} S. Chouridou,¹⁶² Y. S. Chow,¹²⁰ M. C. Chu,^{63a} X. Chu,^{15a} J. Chudoba,¹⁴¹ A. J. Chuinard,¹⁰³ J. J. Chwastowski,⁸⁴ L. Chytka,¹³⁰ D. Cieri,¹¹⁵ K. M. Ciesla,⁸⁴ D. Cinca,⁴⁷ V. Cindro,⁹¹ I. A. Cioară,^{27b} A. Ciocio,¹⁸ F. Ciroto,^{69a,69b} Z. H. Citron,^{180,k} M. Citterio,^{68a} D. A. Ciubotaru,^{27b} B. M. Ciungu,¹⁶⁷ A. Clark,⁵⁴ M. R. Clark,³⁹ P. J. Clark,⁵⁰ C. Clement,^{45a,45b} Y. Coadou,¹⁰¹ M. Cobal,^{66a,66c} A. Coccaro,^{55b} J. Cochran,⁷⁸ H. Cohen,¹⁶¹ A. E. C. Coimbra,³⁶ L. Colasurdo,¹¹⁹ B. Cole,³⁹ A. P. Colijn,¹²⁰ J. Collot,⁵⁸ P. Conde Muñio,^{140a,f} E. Coniavitis,⁵² S. H. Connell,^{33b} I. A. Connelly,⁵⁷ S. Constantinescu,^{27b} F. Conventi,^{69a,ay} A. M. Cooper-Sarkar,¹³⁵ F. Cormier,¹⁷⁵ K. J. R. Cormier,¹⁶⁷ L. D. Corpe,⁹⁴ M. Corradi,^{72a,72b} E. E. Corrigan,⁹⁶ F. Corriveau,^{103,ae} A. S. Cortes-Gonzalez,³⁶ M. J. Costa,¹⁷⁴ F. Costanza,⁵ D. Costanzo,¹⁴⁹ G. Cowan,⁹³ J. W. Cowley,³² J. Crane,¹⁰⁰ K. Cranmer,¹²⁴ S. J. Crawley,⁵⁷ R. A. Creager,¹³⁷ S. Crépe-Renaudin,⁵⁸ F. Crescioli,¹³⁶ M. R. Cristinziani,²⁴ V. Croft,¹²⁰ G. Crosetti,^{41b,41a} A. Cueto,⁵ T. Cuhadar Donszelmann,¹⁴⁹ A. R. Cukierman,¹⁵³ W. R. Cunningham,⁵⁷ S. Czekierda,⁸⁴ P. Czodrowski,³⁶ M. J. Da Cunha Sargedas De Sousa,^{60b} J. V. Da Fonseca Pinto,^{80b} C. Da Via,¹⁰⁰ W. Dabrowski,^{83a} T. Dado,^{28a} S. Dahbi,^{35e} T. Dai,¹⁰⁵ C. Dallapiccola,¹⁰² M. Dam,⁴⁰ G. D'amen,²⁹ V. D'Amico,^{74a,74b} J. Damp,⁹⁹ J. R. Dandoy,¹³⁷ M. F. Daneri,³⁰ N. P. Dang,^{181,j} N. S. Dann,¹⁰⁰ M. Danninger,¹⁷⁵ V. Dao,³⁶ G. Darbo,^{55b} O. Dartsis,⁵ A. Dattagupta,¹³¹ T. Daubney,⁴⁶ S. D'Auria,^{68a,68b} W. Davey,²⁴ C. David,⁴⁶ T. Davidek,¹⁴³ D. R. Davis,⁴⁹ I. Dawson,¹⁴⁹ K. De,⁸ R. De Asmundis,^{69a} M. De Beurs,¹²⁰ S. De Castro,^{23b,23a} S. De Cecco,^{72a,72b} N. De Groot,¹¹⁹ P. de Jong,¹²⁰ H. De la Torre,¹⁰⁶ A. De Maria,^{15c} D. De Pedis,^{72a} A. De Salvo,^{72a} U. De Sanctis,^{73a,73b} M. De Santis,^{73a,73b} A. De Santo,¹⁵⁶ K. De Vasconcelos Corga,¹⁰¹ J. B. De Vivie De Regie,¹³² C. Debenedetti,¹⁴⁶ D. V. Dedovich,⁷⁹ A. M. Deiana,⁴² M. Del Gaudio,^{41b,41a} J. Del Peso,⁹⁸ Y. Delabat Diaz,⁴⁶ D. Delgove,¹³² F. Deliot,^{145,r} C. M. Delitzsch,⁷ M. Della Pietra,^{69a,69b} D. Della Volpe,⁵⁴ A. Dell'Acqua,³⁶ L. Dell'Asta,^{73a,73b} M. Delmastro,⁵ C. Delporte,¹³² P. A. Delsart,⁵⁸ D. A. DeMarco,¹⁶⁷ S. Demers,¹⁸³ M. Demichev,⁷⁹ G. Demontigny,¹⁰⁹ S. P. Denisov,¹²³ D. Denysiuk,¹²⁰ L. D'Eramo,¹³⁶ D. Derendarz,⁸⁴ J. E. Derkaoui,^{35d} F. Derue,¹³⁶ P. Dervan,⁹⁰ K. Desch,²⁴ C. Deterre,⁴⁶ K. Dette,¹⁶⁷ C. Deutsch,²⁴ M. R. Devesa,³⁰ P. O. Deviveiros,³⁶ A. Dewhurst,¹⁴⁴ F. A. Di Bello,⁵⁴ A. Di Ciaccio,^{73a,73b} L. Di Ciaccio,⁵ W. K. Di Clemente,¹³⁷ C. Di Donato,^{69a,69b} A. Di Girolamo,³⁶ G. Di Gregorio,^{71a,71b} B. Di Micco,^{74a,74b} R. Di Nardo,¹⁰² K. F. Di Petrillo,⁵⁹ R. Di Sipio,¹⁶⁷ D. Di Valentino,³⁴ C. Diaconu,¹⁰¹ F. A. Dias,⁴⁰ T. Dias Do Vale,^{140a} M. A. Diaz,^{147a} J. Dickinson,¹⁸ E. B. Diehl,¹⁰⁵ J. Dietrich,¹⁹ S. Díez Cornell,⁴⁶ A. Dimitrievska,¹⁸ W. Ding,^{15b} J. Dingfelder,²⁴ F. Dittus,³⁶ F. Djama,¹⁰¹ T. Djobava,^{159b} J. I. Djuvsland,¹⁷ M. A. B. Do Vale,^{80c} M. Dobre,^{27b} D. Dodsworth,²⁶ C. Doglioni,⁹⁶ J. Dolejsi,¹⁴³ Z. Dolezal,¹⁴³ M. Donadelli,^{80d} B. Dong,^{60c} J. Donini,³⁸ A. D'onofrio,⁹² M. D'Onofrio,⁹⁰ J. Dopke,¹⁴⁴ A. Doria,^{69a} M. T. Dova,⁸⁸ A. T. Doyle,⁵⁷ E. Drechsler,¹⁵² E. Dreyer,¹⁵² T. Dreyer,⁵³ A. S. Drobac,¹⁷⁰ D. Du,^{60b} Y. Duan,^{60b} F. Dubinin,¹¹⁰ M. Dubovsky,^{28a} A. Dubreuil,⁵⁴ E. Duchovni,¹⁸⁰ G. Duckeck,¹¹⁴ A. Ducourthial,¹³⁶ O. A. Ducu,¹⁰⁹ D. Duda,¹¹⁵ A. Dudarev,³⁶ A. C. Dudder,⁹⁹ E. M. Duffield,¹⁸ L. Duflot,¹³² M. Dührssen,³⁶ C. Dülsen,¹⁸² M. Dumancic,¹⁸⁰ A. E. Dumitriu,^{27b} A. K. Duncan,⁵⁷ M. M. Dunford,^{61a} A. Duperrin,¹⁰¹ H. Duran Yildiz,^{4a} M. Düren,⁵⁶ A. Durglishvili,^{159b} D. Duschinger,⁴⁸ B. Dutta,⁴⁶ D. Duvnjak,¹ G. I. Dyckes,¹³⁷ M. Dyndal,³⁶ S. Dysch,¹⁰⁰ B. S. Dziedzic,⁸⁴ K. M. Ecker,¹¹⁵ R. C. Edgar,¹⁰⁵ M. G. Eggleston,⁴⁹ T. Eifert,³⁶ G. Eigen,¹⁷ K. Einsweiler,¹⁸ T. Ekelof,¹⁷² H. El Jarrari,^{35e} M. El Kacimi,^{35c} R. El Kosseifi,¹⁰¹ V. Ellajosyula,¹⁷² M. Ellert,¹⁷² F. Ellinghaus,¹⁸² A. A. Elliot,⁹² N. Ellis,³⁶ J. Elmsheuser,²⁹ M. Elsing,³⁶ D. Emeliyanov,¹⁴⁴ A. Emerman,³⁹ Y. Enari,¹⁶³ M. B. Epland,⁴⁹ J. Erdmann,⁴⁷ A. Ereditato,²⁰ M. Errenst,³⁶ M. Escalier,¹³² C. Escobar,¹⁷⁴ O. Estrada Pastor,¹⁷⁴ E. Etzion,¹⁶¹ H. Evans,⁶⁵ A. Ezhilov,¹³⁸ F. Fabbri,⁵⁷ L. Fabbri,^{23b,23a} V. Fabiani,¹¹⁹ G. Facini,⁹⁴ R. M. Faisca Rodrigues Pereira,^{140a} R. M. Fakhruddinov,¹²³ S. Falciano,^{72a} P. J. Falke,⁵ S. Falke,⁵ J. Faltova,¹⁴³ Y. Fang,^{15a} Y. Fang,^{15a} G. Fanourakis,⁴⁴ M. Fanti,^{68a,68b} M. Faraj,^{66a,66c,u} A. Farbin,⁸ A. Farilla,^{74a} E. M. Farina,^{70a,70b} T. Farooque,¹⁰⁶ S. Farrell,¹⁸ S. M. Farrington,⁵⁰ P. Farthouat,³⁶ F. Fassi,^{35e} P. Fassnacht,³⁶ D. Fassouliotis,⁹ M. Fauci Giannelli,⁵⁰ W. J. Fawcett,³² L. Fayard,¹³² O. L. Fedin,^{138,p} W. Fedorko,¹⁷⁵ M. Feickert,⁴² L. Feligioni,¹⁰¹ A. Fell,¹⁴⁹ C. Feng,^{60b} E. J. Feng,³⁶ M. Feng,⁴⁹ M. J. Fenton,⁵⁷ A. B. Fenyuk,¹²³ J. Ferrando,⁴⁶ A. Ferrante,¹⁷³ A. Ferrari,¹⁷² P. Ferrari,¹²⁰ R. Ferrari,^{70a} D. E. Ferreira de Lima,^{61b} A. Ferrer,¹⁷⁴ D. Ferrere,⁵⁴ C. Ferretti,¹⁰⁵ F. Fiedler,⁹⁹ A. Filipčič,⁹¹ F. Filthaut,¹¹⁹ K. D. Finelli,²⁵ M. C. N. Fiolhais,^{140a,140c,a} L. Fiorini,¹⁷⁴ F. Fischer,¹¹⁴ W. C. Fisher,¹⁰⁶

- I. Fleck,¹⁵¹ P. Fleischmann,¹⁰⁵ R. R. M. Fletcher,¹³⁷ T. Flick,¹⁸² B. M. Flierl,¹¹⁴ L. Flores,¹³⁷ L. R. Flores Castillo,^{63a} F. M. Follega,^{75a,75b} N. Fomin,¹⁷ J. H. Foo,¹⁶⁷ G. T. Forcolin,^{75a,75b} A. Formica,¹⁴⁵ F. A. Förster,¹⁴ A. C. Forti,¹⁰⁰ A. G. Foster,²¹ M. G. Foti,¹³⁵ D. Fournier,¹³² H. Fox,⁸⁹ P. Francavilla,^{71a,71b} S. Francescato,^{72a,72b} M. Franchini,^{23b,23a} S. Franchino,^{61a} D. Francis,³⁶ L. Franconi,²⁰ M. Franklin,⁵⁹ A. N. Fray,⁹² P. M. Freeman,²¹ B. Freund,¹⁰⁹ W. S. Freund,^{80b} E. M. Freundlich,⁴⁷ D. C. Frizzell,¹²⁸ D. Froidevaux,³⁶ J. A. Frost,¹³⁵ C. Fukunaga,¹⁶⁴ E. Fullana Torregrosa,¹⁷⁴ E. Fumagalli,^{55b,55a} T. Fusayasu,¹¹⁶ J. Fuster,¹⁷⁴ A. Gabrielli,^{23b,23a} A. Gabrielli,¹⁸ G. P. Gach,^{83a} S. Gadatsch,⁵⁴ P. Gadow,¹¹⁵ G. Gagliardi,^{55b,55a} L. G. Gagnon,¹⁰⁹ C. Galea,^{27b} B. Galhardo,^{140a} G. E. Gallardo,¹³⁵ E. J. Gallas,¹³⁵ B. J. Gallop,¹⁴⁴ G. Galster,⁴⁰ R. Gamboa Goni,⁹² K. K. Gan,¹²⁶ S. Ganguly,¹⁸⁰ J. Gao,^{60a} Y. Gao,⁵⁰ Y. S. Gao,^{31,m} C. García,¹⁷⁴ J. E. García Navarro,¹⁷⁴ J. A. García Pascual,^{15a} C. Garcia-Argos,⁵² M. Garcia-Sciveres,¹⁸ R. W. Gardner,³⁷ N. Garelli,¹⁵³ S. Gargiulo,⁵² V. Garonne,¹³⁴ A. Gaudiello,^{55b,55a} G. Gaudio,^{70a} I. L. Gavrilenko,¹¹⁰ A. Gavriluk,¹¹¹ C. Gay,¹⁷⁵ G. Gaycken,⁴⁶ E. N. Gazis,¹⁰ A. A. Geanta,^{27b} C. M. Gee,¹⁴⁶ C. N. P. Gee,¹⁴⁴ J. Geisen,⁵³ M. Geisen,⁹⁹ M. P. Geisler,^{61a} C. Gemme,^{55b} M. H. Genest,⁵⁸ C. Geng,¹⁰⁵ S. Gentile,^{72a,72b} S. George,⁹³ T. Gerialis,⁴⁴ L. O. Gerlach,⁵³ P. Gessinger-Befurt,⁹⁹ G. Gessner,⁴⁷ S. Ghasemi,¹⁵¹ M. Ghasemi Bostanabad,¹⁷⁶ A. Ghosh,¹³² A. Ghosh,⁷⁷ B. Giacobbe,^{23b} S. Giagu,^{72a,72b} N. Giangiacomi,^{23b,23a} P. Giannetti,^{71a} A. Giannini,^{69a,69b} G. Giannini,¹⁴ S. M. Gibson,⁹³ M. Gignac,¹⁴⁶ D. Gillberg,³⁴ G. Gilles,¹⁸² D. M. Gingrich,^{3,ax} M. P. Giordani,^{66a,66c} F. M. Giorgi,^{23b} P. F. Giraud,¹⁴⁵ G. Giugliarelli,^{66a,66c} D. Giugni,^{68a} F. Giuli,^{73a,73b} S. Gkaitatzis,¹⁶² I. Gkiyalas,^{9,h} E. L. Gkoukousis,¹⁴ P. Gkoutoumis,¹⁰ L. K. Gladilin,¹¹³ C. Glasman,⁹⁸ J. Glatzer,¹⁴ P. C. F. Glaysher,⁴⁶ A. Glazov,⁴⁶ G. R. Gledhill,¹³¹ M. Goblirsch-Kolb,²⁶ D. Godin,¹⁰⁹ S. Goldfarb,¹⁰⁴ T. Golling,⁵⁴ D. Golubkov,¹²³ A. Gomes,^{140a,140b} R. Goncalves Gama,⁵³ R. Gonçalo,^{140a,140b} G. Gonella,⁵² L. Gonella,²¹ A. Gongadze,⁷⁹ F. Gonnella,²¹ J. L. Gonski,⁵⁹ S. González de la Hoz,¹⁷⁴ S. Gonzalez-Sevilla,⁵⁴ G. R. Gonzalvo Rodriguez,¹⁷⁴ L. Goossens,³⁶ P. A. Gorbounov,¹¹¹ H. A. Gordon,²⁹ B. Gorini,³⁶ E. Gorini,^{67a,67b} A. Gorišek,⁹¹ A. T. Goshaw,⁴⁹ M. I. Gostkin,⁷⁹ C. A. Gottardo,¹¹⁹ M. Gouighri,^{35b} D. Goujdami,^{35c} A. G. Goussiou,¹⁴⁸ N. Govender,^{33b} C. Goy,⁵ E. Gozani,¹⁶⁰ I. Grabowska-Bold,^{83a} E. C. Graham,⁹⁰ J. Gramling,¹⁷¹ E. Gramstad,¹³⁴ S. Grancagnolo,¹⁹ M. Grandi,¹⁵⁶ V. Gratchev,¹³⁸ P. M. Gravila,^{27f} F. G. Gravili,^{67a,67b} C. Gray,⁵⁷ H. M. Gray,¹⁸ C. Greife,²⁴ K. Gregersen,⁹⁶ I. M. Gregor,⁴⁶ P. Grenier,¹⁵³ K. Grevtsov,⁴⁶ C. Grieco,¹⁴ N. A. Grieser,¹²⁸ J. Griffiths,⁸ A. A. Grillo,¹⁴⁶ K. Grimm,^{31,1} S. Grinstein,^{14,z} J.-F. Grivaz,¹³² S. Groh,⁹⁹ E. Cross,¹⁸⁰ J. Grosse-Knetter,⁵³ Z. J. Grout,⁹⁴ C. Grud,¹⁰⁵ A. Grummer,¹¹⁸ L. Guan,¹⁰⁵ W. Guan,¹⁸¹ J. Guenther,³⁶ A. Guerguichon,¹³² J. G. R. Guerrero Rojas,¹⁷⁴ F. Guescini,¹¹⁵ D. Guest,¹⁷¹ R. Gugel,⁵² T. Guillemin,⁵ S. Guindon,³⁶ U. Gul,⁵⁷ J. Guo,^{60c} W. Guo,¹⁰⁵ Y. Guo,^{60a,t} Z. Guo,¹⁰¹ R. Gupta,⁴⁶ S. Gurbuz,^{12c} G. Gustavino,¹²⁸ M. Guth,⁵² P. Gutierrez,¹²⁸ C. Gutsche,⁹⁴ C. Guyot,¹⁴⁵ C. Gwenlan,¹³⁵ C. B. Gwilliam,⁹⁰ A. Haas,¹²⁴ C. Haber,¹⁸ H. K. Hadavand,⁸ N. Haddad,^{35e} A. Hadeef,^{60a} S. Hageböck,³⁶ M. Haleem,¹⁷⁷ J. Haley,¹²⁹ G. Halladjian,¹⁰⁶ G. D. Hallewell,¹⁰¹ K. Hamacher,¹⁸² P. Hamal,¹³⁰ K. Hamano,¹⁷⁶ H. Hamdaoui,^{35c} G. N. Hamity,¹⁴⁹ K. Han,^{60a,ak} L. Han,^{60a} S. Han,^{15a,15d} Y. F. Han,¹⁶⁷ K. Hanagaki,^{81,x} M. Hance,¹⁴⁶ D. M. Handl,¹¹⁴ B. Haney,¹³⁷ R. Hankache,¹³⁶ E. Hansen,⁹⁶ J. B. Hansen,⁴⁰ J. D. Hansen,⁴⁰ M. C. Hansen,²⁴ P. H. Hansen,⁴⁰ E. C. Hanson,¹⁰⁰ K. Hara,¹⁶⁹ T. Harenberg,¹⁸² S. Harkusha,¹⁰⁷ P. F. Harrison,¹⁷⁸ N. M. Hartmann,¹¹⁴ Y. Hasegawa,¹⁵⁰ A. Hasib,⁵⁰ S. Hassani,¹⁴⁵ S. Haug,²⁰ R. Hauser,¹⁰⁶ L. B. Havener,³⁹ M. Havranek,¹⁴² C. M. Hawkes,²¹ R. J. Hawkins,³⁶ D. Hayden,¹⁰⁶ C. Hayes,¹⁵⁵ R. L. Hayes,¹⁷⁵ C. P. Hays,¹³⁵ J. M. Hays,⁹² H. S. Hayward,⁹⁰ S. J. Hayward,¹⁴⁴ F. He,^{60a} M. P. Heath,⁵⁰ V. Hedberg,⁹⁶ L. Heelan,⁸ S. Heer,²⁴ K. K. Heidegger,⁵² W. D. Heidorn,⁷⁸ J. Heilman,³⁴ S. Heim,⁴⁶ T. Heim,¹⁸ B. Heinemann,^{46,as} J. J. Heinrich,¹³¹ L. Heinrich,³⁶ C. Heinz,⁵⁶ J. Hejbal,¹⁴¹ L. Helary,^{61b} A. Held,¹⁷⁵ S. Hellesund,¹³⁴ C. M. Helling,¹⁴⁶ S. Hellman,^{45a,45b} C. Helsens,³⁶ R. C. W. Henderson,⁸⁹ Y. Heng,¹⁸¹ S. Henkelmann,¹⁷⁵ A. M. Henriques Correia,³⁶ G. H. Herbert,¹⁹ H. Herde,²⁶ V. Herget,¹⁷⁷ Y. Hernández Jiménez,^{33c} H. Herr,⁹⁹ M. G. Herrmann,¹¹⁴ T. Herrmann,⁴⁸ G. Herten,⁵² R. Hertenberger,¹¹⁴ L. Hervas,³⁶ T. C. Herwig,¹³⁷ G. G. Hesketh,⁹⁴ N. P. Hesse,^{168a} A. Higashida,¹⁶³ S. Higashino,⁸¹ E. Higón-Rodríguez,¹⁷⁴ K. Hildebrand,³⁷ E. Hill,¹⁷⁶ J. C. Hill,³² K. K. Hill,²⁹ K. H. Hiller,⁴⁶ S. J. Hillier,²¹ M. Hils,⁴⁸ I. Hinchliffe,¹⁸ F. Hinterkeuser,²⁴ M. Hirose,¹³³ S. Hirose,⁵² D. Hirschbuehl,¹⁸² B. Hiti,⁹¹ O. Hladik,¹⁴¹ D. R. Hlaluku,^{33c} X. Hoad,⁵⁰ J. Hobbs,¹⁵⁵ N. Hod,¹⁸⁰ M. C. Hodgkinson,¹⁴⁹ A. Hoecker,³⁶ F. Hoenic,¹¹⁴ D. Hohn,⁵² D. Hohov,¹³² T. R. Holmes,³⁷ M. Holzbock,¹¹⁴ L. B. A. H. Hommels,³² S. Honda,¹⁶⁹ T. M. Hong,¹³⁹ J. C. Honig,⁵² A. Hönle,¹¹⁵ B. H. Hooberman,¹⁷³ W. H. Hopkins,⁶ Y. Horii,¹¹⁷ P. Horn,⁴⁸ L. A. Horyn,³⁷ S. Hou,¹⁵⁸ A. Hoummada,^{35a} J. Howarth,¹⁰⁰ J. Hoya,⁸⁸ M. Hrabovsky,¹³⁰ J. Hrdinka,⁷⁶ I. Hristova,¹⁹ J. Hrivnac,¹³² A. Hrynevich,¹⁰⁸ T. Hryn'ova,⁵ P. J. Hsu,⁶⁴ S.-C. Hsu,¹⁴⁸ Q. Hu,²⁹ S. Hu,^{60c} Y. F. Hu,^{15a} D. P. Huang,⁹⁴ Y. Huang,^{60a} Y. Huang,^{15a} Z. Hubacek,¹⁴² F. Hubaut,¹⁰¹ M. Huebner,²⁴ F. Huegging,²⁴ T. B. Huffman,¹³⁵ M. Huhtinen,³⁶ R. F. H. Hunter,³⁴ P. Huo,¹⁵⁵ A. M. Hupe,³⁴ N. Huseynov,^{79,ag} J. Huston,¹⁰⁶ J. Huth,⁵⁹ R. Hyneman,¹⁰⁵ S. Hyrych,^{28a} G. Iacobucci,⁵⁴ G. Iakovidis,²⁹ I. Ibragimov,¹⁵¹ L. Iconomidou-Fayard,¹³² Z. Idrissi,^{35e} P. Ingo,³⁶ R. Ignazzi,⁴⁰ O. Igonkina,^{120,ab,*} R. Iguchi,¹⁶³ T. Iizawa,⁵⁴ Y. Ikegami,⁸¹ M. Ikeno,⁸¹ D. Iliadis,¹⁶² N. Ilic,^{119,167,ae} F. Iltzsche,⁴⁸ G. Introzzi,^{70a,70b} M. Iodice,^{74a} K. Iordanidou,^{168a} V. Ippolito,^{72a,72b} M. F. Isacson,¹⁷² M. Ishino,¹⁶³ W. Islam,¹²⁹ C. Issever,¹³⁵ S. Istin,¹⁶⁰ F. Ito,¹⁶⁹ J. M. Iturbe Ponce,^{63a} R. Iuppa,^{75a,75b} A. Ivina,¹⁸⁰ H. Iwasaki,⁸¹ J. M. Izen,⁴³ V. Izzo,^{69a} P. Jacka,¹⁴¹ P. Jackson,¹ R. M. Jacobs,²⁴ B. P. Jaeger,¹⁵² V. Jain,² G. Jäkel,¹⁸² K. B. Jakobi,⁹⁹ K. Jakobs,⁵² S. Jakobsen,⁷⁶ T. Jakoubek,¹⁴¹ J. Jamieson,⁵⁷ K. W. Janas,^{83a} R. Jansky,⁵⁴ J. Janssen,²⁴ M. Janus,⁵³ P. A. Janus,^{83a} G. Jarlskog,⁹⁶ N. Javadov,^{79,ag} T. Javůrek,³⁶ M. Javurkova,⁵² F. Jeanneau,¹⁴⁵ L. Jeanty,¹³¹ J. Jejelava,^{159a,ah} A. Jelinskas,¹⁷⁸ P. Jenni,^{52,b} J. Jeong,⁴⁶ N. Jeong,⁴⁶ S. Jézéquel,⁵ H. Ji,¹⁸¹ J. Jia,¹⁵⁵ H. Jiang,⁷⁸ Y. Jiang,^{60a} Z. Jiang,^{153,q} S. Jiggins,⁵² F. A. Jimenez Morales,³⁸ J. Jimenez Pena,¹¹⁵ S. Jin,^{15c} A. Jinaru,^{27b} O. Jinnouchi,¹⁶⁵ H. Jivan,^{33c} P. Johansson,¹⁴⁹ K. A. Johns,⁷ C. A. Johnson,⁶⁵ K. Jon-And,^{45a,45b} R. W. L. Jones,⁸⁹ S. D. Jones,¹⁵⁶ S. Jones,⁷ T. J. Jones,⁹⁰ J. Jongmanns,^{61a} P. M. Jorge,^{140a} J. Jovicevic,³⁶ X. Ju,¹⁸ J. J. Jungbunrath,¹¹⁵ A. Juste Rozas,^{14,z} A. Kaczmarska,⁸⁴ M. Kado,^{72a,72b} H. Kagan,¹²⁶

J. Terron,⁹⁸ S. Terzo,¹⁴ M. Testa,⁵¹ R. J. Teuscher,^{167,ae} S. J. Thais,¹⁸³ T. Theveneaux-Pelzer,⁴⁶ F. Thiele,⁴⁰ D. W. Thomas,⁹³ J. O. Thomas,⁴² J. P. Thomas,²¹ A. S. Thompson,⁵⁷ P. D. Thompson,²¹ L. A. Thomsen,¹⁸³ E. Thomson,¹³⁷ E. J. Thorpe,⁹² R. E. Ticse Torres,⁵³ V. O. Tikhomirov,^{110,ap} Yu. A. Tikhonov,^{122b,122a} S. Timoshenko,¹¹² P. Tipton,¹⁸³ S. Tisserant,¹⁰¹ K. Todome,^{23b,23a} S. Todorova-Nova,⁵ S. Todt,⁴⁸ J. Tojo,⁸⁷ S. Tokár,^{28a} K. Tokushuku,⁸¹ E. Tolley,¹²⁶ K. G. Tomiwa,^{33c} M. Tomoto,¹¹⁷ L. Tompkins,^{153,q} B. Tong,⁵⁹ P. Tornambe,¹⁰² E. Torrence,¹³¹ H. Torres,⁴⁸ E. Torr  Pastor,¹⁴⁸ C. Tosciri,¹³⁵ J. Toth,^{101,ad} D. R. Tovey,¹⁴⁹ A. Traet,¹⁷ C. J. Treado,¹²⁴ T. Trefzger,¹⁷⁷ F. Tresoldi,¹⁵⁶ A. Tricoli,²⁹ I. M. Trigger,^{168a} S. Trincz-Duvoid,¹³⁶ W. Trischuk,¹⁶⁷ B. Trocm ,⁵⁸ A. Trofymov,¹⁴⁵ C. Troncon,^{68a} M. Trovatelli,¹⁷⁶ F. Trovato,¹⁵⁶ L. Truong,^{33b} M. Trzebinski,⁸⁴ A. Trzupek,⁸⁴ F. Tsai,⁴⁶ J. C-L. Tseng,¹³⁵ P. V. Tsiarshka,^{107,aj} A. Tsirigotis,¹⁶² V. Tsiskaridze,¹⁵⁵ E. G. Tskhadadze,^{159a} M. Tsopoulou,¹⁶² I. I. Tsukerman,¹¹¹ V. Tsulaia,¹⁸ S. Tsuno,⁸¹ D. Tsybychev,¹⁵⁵ Y. Tu,^{63b} A. Tudorache,^{27b} V. Tudorache,^{27b} T. T. Tulbure,^{27a} A. N. Tuna,⁵⁹ S. Turchikhin,⁷⁹ D. Turgeman,¹⁸⁰ I. Turk Cakir,^{4b,w} R. J. Turner,²¹ R. T. Turra,^{68a} P. M. Tuts,³⁹ S. Tzamarias,¹⁶² E. Tzovara,⁹⁹ G. Ucchielli,⁴⁷ K. Uchida,¹⁶³ I. Ueda,⁸¹ M. Ughetto,^{45a,45b} F. Ukegawa,¹⁶⁹ G. Unal,³⁶ A. Undrus,²⁹ G. Unel,¹⁷¹ F. C. Ungaro,¹⁰⁴ Y. Unno,⁸¹ K. Uno,¹⁶³ J. Urban,^{28b} P. Urquijo,¹⁰⁴ G. Usai,⁸ Z. Uysal,^{12d} L. Vacavant,¹⁰¹ V. Vacek,¹⁴² B. Vachon,¹⁰³ K. O. H. Vadla,¹³⁴ A. Vaidya,⁹⁴ C. Valderanis,¹¹⁴ E. Valdes Santurio,^{45a,45b} M. Valente,⁵⁴ S. Valentinetti,^{23b,23a} A. Valero,¹⁷⁴ L. Val ry,⁴⁶ R. A. Vallance,²¹ A. Vallier,³⁶ J. A. Valls Ferrer,¹⁷⁴ T. R. Van Daalen,¹⁴ P. Van Gemmeren,⁶ I. Van Vulpen,¹²⁰ M. Vanadia,^{73a,73b} W. Vandelli,³⁶ E. R. Vandewall,¹²⁹ A. Vaniachine,¹⁶⁶ D. Vannicola,^{72a,72b} R. Vari,^{72a} E. W. Varnes,⁷ C. Varni,^{55b,55a} T. Varol,¹⁵⁸ D. Varouchas,¹³² K. E. Varvell,¹⁵⁷ M. E. Vasile,^{27b} G. A. Vasquez,¹⁷⁶ J. G. Vasquez,¹⁸³ F. Vazeille,³⁸ D. Vazquez Furelos,¹⁴ T. Vazquez Schroeder,³⁶ J. Veatch,⁵³ V. Vecchio,^{74a,74b} M. J. Veen,¹²⁰ L. M. Veloce,¹⁶⁷ F. Veloso,^{140a,140c} S. Veneziano,^{72a} A. Ventura,^{67a,67b} N. Venturi,³⁶ A. Verbytskyi,¹¹⁵ V. Vercesi,^{70a} M. Verducci,^{71a,71b} C. M. Vergel Infante,⁷⁸ C. Vergis,²⁴ W. Verkerke,¹²⁰ A. T. Vermeulen,¹²⁰ J. C. Vermeulen,¹²⁰ M. C. Vetterli,^{152,ax} N. Viaux Maira,^{147b} M. Vicente Barreto Pinto,⁵⁴ T. Vickey,¹⁴⁹ O. E. Vickey Boeriu,¹⁴⁹ G. H. A. Viehhauser,¹³⁵ L. Vigani,^{61b} M. Villa,^{23b,23a} M. Villaplana Perez,^{68a,68b} E. Vilucchi,⁵¹ M. G. Vincter,³⁴ G. S. Virdee,²¹ A. Vishwakarma,⁴⁶ C. Vittori,^{23b,23a} I. Vivarelli,¹⁵⁶ M. Vogel,¹⁸² P. Vokac,¹⁴² S. E. von Buddenbrock,^{33c} E. Von Toerne,²⁴ V. Vorobel,¹⁴³ K. Vorobev,¹¹² M. Vos,¹⁷⁴ J. H. Vossebeld,⁹⁰ M. Vozak,¹⁰⁰ N. Vranjes,¹⁶ M. Vranjes Milosavljevic,¹⁶ V. Vrba,¹⁴² M. Vreeswijk,¹²⁰ R. Vuillermet,³⁶ I. Vukotic,³⁷ P. Wagner,²⁴ W. Wagner,¹⁸² J. Wagner-Kuhr,¹¹⁴ S. Wahdan,¹⁸² H. Wahlberg,⁸⁸ V. M. Walbrecht,¹¹⁵ J. Walder,⁸⁹ R. Walker,¹¹⁴ S. D. Walker,⁹³ W. Walkowiak,¹⁵¹ V. Wallangen,^{45a,45b} A. M. Wang,⁵⁹ C. Wang,^{60c} C. Wang,^{60b} F. Wang,¹⁸¹ H. Wang,¹⁸ H. Wang,³ J. Wang,^{63a} J. Wang,¹⁵⁷ J. Wang,^{61b} P. Wang,⁴² Q. Wang,¹²⁸ R.-J. Wang,⁹⁹ R. Wang,^{60a} R. Wang,⁶ S. M. Wang,¹⁵⁸ W. T. Wang,^{60a} W. Wang,^{15c,af} W. X. Wang,^{60a,af} Y. Wang,^{60a,am} Z. Wang,^{60c} C. Wanotayaroj,⁴⁶ A. Warburton,¹⁰³ C. P. Ward,³² D. R. Wardrope,⁹⁴ N. Warrack,⁵⁷ A. Washbrook,⁵⁰ A. T. Watson,²¹ M. F. Watson,²¹ G. Watts,¹⁴⁸ B. M. Waugh,⁹⁴ A. F. Webb,¹¹ S. Webb,⁹⁹ C. Weber,¹⁸³ M. S. Weber,²⁰ S. A. Weber,³⁴ S. M. Weber,^{61a} A. R. Weidberg,¹³⁵ J. Weingarten,⁴⁷ M. Weirich,⁹⁹ C. Weiser,⁵² P. S. Wells,³⁶ T. Wenaus,²⁹ T. Wengler,³⁶ S. Wenig,³⁶ N. Wermes,²⁴ M. D. Werner,⁷⁸ M. Wessels,^{61a} T. D. Weston,²⁰ K. Whalen,¹³¹ N. L. Whallon,¹⁴⁸ A. M. Wharton,⁸⁹ A. S. White,¹⁰⁵ A. White,⁸ M. J. White,¹ D. Whiteson,¹⁷¹ B. W. Whitmore,⁸⁹ W. Wiedenmann,¹⁸¹ M. Wielers,¹⁴⁴ N. Wieseotte,⁹⁹ C. Wiglesworth,⁴⁰ L. A. M. Wiik-Fuchs,⁵² F. Wilk,¹⁰⁰ H. G. Wilkens,³⁶ L. J. Wilkins,⁹³ H. H. Williams,¹³⁷ S. Williams,³² C. Willis,¹⁰⁶ S. Willocq,¹⁰² J. A. Wilson,²¹ I. Wingerter-Seez,⁵ E. Winkels,¹⁵⁶ F. Winklmeier,¹³¹ O. J. Winston,¹⁵⁶ B. T. Winter,⁵² M. Wittgen,¹⁵³ M. Wobisch,⁹⁵ A. Wolf,⁹⁹ T. M. H. Wolf,¹²⁰ R. Wolff,¹⁰¹ R. W. W lker,¹³⁵ J. Wollrath,⁵² M. W. Wolter,⁸⁴ H. Wolters,^{140a,140c} V. W. S. Wong,¹⁷⁵ N. L. Woods,¹⁴⁶ S. D. Worm,²¹ B. K. Wosiek,⁸⁴ K. W. Woźniak,⁸⁴ K. Wraight,⁵⁷ S. L. Wu,¹⁸¹ X. Wu,⁵⁴ Y. Wu,^{60a} T. R. Wyatt,¹⁰⁰ B. M. Wynne,⁵⁰ S. Xella,⁴⁰ Z. Xi,¹⁰⁵ L. Xia,¹⁷⁸ X. Xiao,¹⁰⁵ I. Xiotidis,¹⁵⁶ D. Xu,^{15a} H. Xu,^{60a,c} L. Xu,²⁹ T. Xu,¹⁴⁵ W. Xu,¹⁰⁵ Z. Xu,^{60b} Z. Xu,¹⁵³ B. Yabsley,¹⁵⁷ S. Yacoob,^{33a} K. Yajima,¹³³ D. P. Yallup,⁹⁴ D. Yamaguchi,¹⁶⁵ Y. Yamaguchi,¹⁶⁵ A. Yamamoto,⁸¹ M. Yamatani,¹⁶³ T. Yamazaki,¹⁶³ Y. Yamazaki,⁸² Z. Yan,²⁵ H. J. Yang,^{60c,60d} H. T. Yang,¹⁸ S. Yang,⁷⁷ X. Yang,^{60b,58} Y. Yang,¹⁶³ W-M. Yao,¹⁸ Y. C. Yap,⁴⁶ Y. Yasu,⁸¹ E. Yatsenko,^{60c,60d} J. Ye,⁴² S. Ye,²⁹ I. Yeletsikh,⁷⁹ M. R. Yexley,⁸⁹ E. Yigitbasi,²⁵ K. Yorita,¹⁷⁹ K. Yoshihara,¹³⁷ C. J. S. Young,³⁶ C. Young,¹⁵³ J. Yu,⁷⁸ R. Yuan,^{60b,i} X. Yue,^{61a} S. P. Y. Yuen,²⁴ M. Zaazoua,^{35c} B. Zabinski,⁸⁴ G. Zacharis,¹⁰ E. Zaffaroni,⁵⁴ J. Zahreddine,¹³⁶ A. M. Zaitsev,^{123,ao} T. Zakareishvili,^{159b} N. Zakharchuk,³⁴ S. Zambona,⁵⁹ D. Zanzi,³⁶ D. R. Zaripovas,⁵⁷ S. V. Zei ner,⁴⁷ C. Zeitnitz,¹⁸² G. Zemaityte,¹³⁵ J. C. Zeng,¹⁷³ O. Zenin,¹²³ T.  eni ,^{28a} D. Zerwas,¹³² M. Zgubi ,¹³⁵ B. Zhang,^{15c} D. F. Zhang,^{15b} G. Zhang,^{15b} H. Zhang,^{15c} J. Zhang,⁶ L. Zhang,^{15c} L. Zhang,^{60a} M. Zhang,¹⁷³ R. Zhang,²⁴ X. Zhang,^{60b} Y. Zhang,^{15a,15d} Z. Zhang,^{63a} Z. Zhang,¹³² P. Zhao,⁴⁹ Y. Zhao,^{60b} Z. Zhao,^{60a} A. Zhemchugov,⁷⁹ Z. Zheng,¹⁰⁵ D. Zhong,¹⁷³ B. Zhou,¹⁰⁵ C. Zhou,¹⁸¹ M. S. Zhou,^{15a,15d} M. Zhou,¹⁵⁵ N. Zhou,^{60c} Y. Zhou,⁷ C. G. Zhu,^{60b} C. Zhu,^{15a} H. L. Zhu,^{60a} H. Zhu,^{15a} J. Zhu,¹⁰⁵ Y. Zhu,^{60a} X. Zhuang,^{15a} K. Zhukov,¹¹⁰ V. Zhulanov,^{122b,122a} D. Ziemińska,⁶⁵ N. I. Zimine,⁷⁹ S. Zimmermann,⁵² Z. Zinonos,¹¹⁵ M. Ziolkowski,¹⁵¹ L.  ivkovi ,¹⁶ G. Zobernig,¹⁸¹ A. Zoccoli,^{23b,23a} K. Zoch,⁵³ T. G. Zorbas,¹⁴⁹ R. Zou,³⁷ and L. Zwalinski³⁶

(ATLAS Collaboration)

¹Department of Physics, University of Adelaide, Adelaide, Australia²Physics Department, SUNY Albany, Albany, New York, USA³Department of Physics, University of Alberta, Edmonton, Alberta, Canada^{4a}Department of Physics, Ankara University, Ankara, Turkey^{4b}Istanbul Aydin University, Istanbul, Turkey

- ^{4c}*Division of Physics, TOBB University of Economics and Technology, Ankara, Turkey*
- ⁵*LAPP, Université Grenoble Alpes, Université Savoie Mont Blanc, CNRS/IN2P3, Annecy, France*
- ⁶*High Energy Physics Division, Argonne National Laboratory, Argonne, Illinois, USA*
- ⁷*Department of Physics, University of Arizona, Tucson, Arizona, USA*
- ⁸*Department of Physics, University of Texas at Arlington, Arlington, Texas, USA*
- ⁹*Physics Department, National and Kapodistrian University of Athens, Athens, Greece*
- ¹⁰*Physics Department, National Technical University of Athens, Zografou, Greece*
- ¹¹*Department of Physics, University of Texas at Austin, Austin, Texas, USA*
- ^{12a}*Bahcesehir University, Faculty of Engineering and Natural Sciences, Istanbul, Turkey*
- ^{12b}*Istanbul Bilgi University, Faculty of Engineering and Natural Sciences, Istanbul, Turkey*
- ^{12c}*Department of Physics, Bogazici University, Istanbul, Turkey*
- ^{12d}*Department of Physics Engineering, Gaziantep University, Gaziantep, Turkey*
- ¹³*Institute of Physics, Azerbaijan Academy of Sciences, Baku, Azerbaijan*
- ¹⁴*Institut de Física d'Altes Energies (IFAE), Barcelona Institute of Science and Technology, Barcelona, Spain*
- ^{15a}*Institute of High Energy Physics, Chinese Academy of Sciences, Beijing, China*
- ^{15b}*Physics Department, Tsinghua University, Beijing, China*
- ^{15c}*Department of Physics, Nanjing University, Nanjing, China*
- ^{15d}*University of Chinese Academy of Science (UCAS), Beijing, China*
- ¹⁶*Institute of Physics, University of Belgrade, Belgrade, Serbia*
- ¹⁷*Department for Physics and Technology, University of Bergen, Bergen, Norway*
- ¹⁸*Physics Division, Lawrence Berkeley National Laboratory and University of California, Berkeley, California, USA*
- ¹⁹*Institut für Physik, Humboldt Universität zu Berlin, Berlin, Germany*
- ²⁰*Albert Einstein Center for Fundamental Physics and Laboratory for High Energy Physics, University of Bern, Bern, Switzerland*
- ²¹*School of Physics and Astronomy, University of Birmingham, Birmingham, United Kingdom*
- ²²*Facultad de Ciencias y Centro de Investigaciones, Universidad Antonio Nariño, Bogota, Colombia*
- ^{23a}*INFN Bologna and Università di Bologna, Dipartimento di Fisica, Bologna, Italy*
- ^{23b}*INFN Sezione di Bologna, Bologna, Italy*
- ²⁴*Physikalisches Institut, Universität Bonn, Bonn, Germany*
- ²⁵*Department of Physics, Boston University, Boston, Massachusetts, USA*
- ²⁶*Department of Physics, Brandeis University, Waltham, Massachusetts, USA*
- ^{27a}*Transilvania University of Brasov, Brasov, Romania*
- ^{27b}*Horia Hulubei National Institute of Physics and Nuclear Engineering, Bucharest, Romania*
- ^{27c}*Department of Physics, Alexandru Ioan Cuza University of Iasi, Iasi, Romania*
- ^{27d}*National Institute for Research and Development of Isotopic and Molecular Technologies, Physics Department, Cluj-Napoca, Romania*
- ^{27e}*University Politehnica Bucharest, Bucharest, Romania*
- ^{27f}*West University in Timisoara, Timisoara, Romania*
- ^{28a}*Faculty of Mathematics, Physics and Informatics, Comenius University, Bratislava, Slovak Republic*
- ^{28b}*Department of Subnuclear Physics, Institute of Experimental Physics of the Slovak Academy of Sciences, Kosice, Slovak Republic*
- ²⁹*Physics Department, Brookhaven National Laboratory, Upton, New York, USA*
- ³⁰*Departamento de Física, Universidad de Buenos Aires, Buenos Aires, Argentina*
- ³¹*California State University, California, USA*
- ³²*Cavendish Laboratory, University of Cambridge, Cambridge, United Kingdom*
- ^{33a}*Department of Physics, University of Cape Town, Cape Town, South Africa*
- ^{33b}*Department of Mechanical Engineering Science, University of Johannesburg, Johannesburg, South Africa*
- ^{33c}*School of Physics, University of the Witwatersrand, Johannesburg, South Africa*
- ³⁴*Department of Physics, Carleton University, Ottawa, Ontario, Canada*
- ^{35a}*Faculté des Sciences Ain Chock, Réseau Universitaire de Physique des Hautes Energies-Université Hassan II, Casablanca, Morocco*
- ^{35b}*Faculté des Sciences, Université Ibn-Tofail, Kénitra, Morocco*
- ^{35c}*Faculté des Sciences Semlalia, Université Cadi Ayyad, LPHEA-Marrakech, Morocco*
- ^{35d}*Faculté des Sciences, Université Mohamed Premier and LPTPM, Oujda, Morocco*
- ^{35e}*Faculté des sciences, Université Mohammed V, Rabat, Morocco*
- ³⁶*CERN, Geneva, Switzerland*
- ³⁷*Enrico Fermi Institute, University of Chicago, Chicago, Illinois, USA*
- ³⁸*LPC, Université Clermont Auvergne, CNRS/IN2P3, Clermont-Ferrand, France*
- ³⁹*Nevis Laboratory, Columbia University, Irvington, New York, USA*
- ⁴⁰*Niels Bohr Institute, University of Copenhagen, Copenhagen, Denmark*
- ^{41a}*Dipartimento di Fisica, Università della Calabria, Rende, Italy*
- ^{41b}*INFN Gruppo Collegato di Cosenza, Laboratori Nazionali di Frascati, Italy*
- ⁴²*Physics Department, Southern Methodist University, Dallas, Texas, USA*

- ⁴³Physics Department, University of Texas at Dallas, Richardson, Texas, USA
- ⁴⁴National Centre for Scientific Research “Demokritos”, Agia Paraskevi, Greece
- ^{45a}Department of Physics, Stockholm University, Stockholm, Sweden
- ^{45b}Oskar Klein Centre, Stockholm, Sweden
- ⁴⁶Deutsches Elektronen-Synchrotron DESY, Hamburg and Zeuthen, Germany
- ⁴⁷Lehrstuhl für Experimentelle Physik IV, Technische Universität Dortmund, Dortmund, Germany
- ⁴⁸Institut für Kern- und Teilchenphysik, Technische Universität Dresden, Dresden, Germany
- ⁴⁹Department of Physics, Duke University, Durham, North Carolina, USA
- ⁵⁰SUPA (School of Physics and Astronomy), University of Edinburgh, Edinburgh, United Kingdom
- ⁵¹INFN e Laboratori Nazionali di Frascati, Frascati, Italy
- ⁵²Physikalisches Institut, Albert-Ludwigs-Universität Freiburg, Freiburg, Germany
- ⁵³II. Physikalisches Institut, Georg-August-Universität Göttingen, Göttingen, Germany
- ⁵⁴Département de Physique Nucléaire et Corpusculaire, Université de Genève, Geneva, Switzerland
- ^{55a}Dipartimento di Fisica, Università di Genova, Genova, Italy
- ^{55b}INFN Sezione di Genova, Italy
- ⁵⁶II. Physikalisches Institut, Justus-Liebig-Universität Giessen, Giessen, Germany
- ⁵⁷SUPA (School of Physics and Astronomy), University of Glasgow, Glasgow, United Kingdom
- ⁵⁸LPSC, Université Grenoble Alpes, CNRS/IN2P3, Grenoble INP, Grenoble, France
- ⁵⁹Laboratory for Particle Physics and Cosmology, Harvard University, Cambridge, Massachusetts, USA
- ^{60a}Department of Modern Physics and State Key Laboratory of Particle Detection and Electronics, University of Science and Technology of China, Hefei, China
- ^{60b}Institute of Frontier and Interdisciplinary Science and Key Laboratory of Particle Physics and Particle Irradiation (MOE), Shandong University, Qingdao, China
- ^{60c}School of Physics and Astronomy, Shanghai Jiao Tong University, KLPPAC-MoE, SKLPPC, Shanghai, China
- ^{60d}Tsung-Dao Lee Institute, Shanghai, China
- ^{61a}Kirchhoff-Institut für Physik, Ruprecht-Karls-Universität Heidelberg, Heidelberg, Germany
- ^{61b}Physikalisches Institut, Ruprecht-Karls-Universität Heidelberg, Heidelberg, Germany
- ⁶²Faculty of Applied Information Science, Hiroshima Institute of Technology, Hiroshima Japan
- ^{63a}Department of Physics, Chinese University of Hong Kong, Shatin, N.T., Hong Kong, China
- ^{63b}Department of Physics, University of Hong Kong, Hong Kong, China
- ^{63c}Department of Physics and Institute for Advanced Study, Hong Kong University of Science and Technology, Clear Water Bay, Kowloon, Hong Kong, China
- ⁶⁴Department of Physics, National Tsing Hua University, Hsinchu, Taiwan
- ⁶⁵Department of Physics, Indiana University, Bloomington, Indiana, USA
- ^{66a}INFN Gruppo Collegato di Udine, Sezione di Trieste, Udine, Italy
- ^{66b}ICTP, Trieste, Italy
- ^{66c}Dipartimento Politecnico di Ingegneria e Architettura, Università di Udine, Udine, Italy
- ^{67a}INFN Sezione di Lecce, Lecce, Italy
- ^{67b}Dipartimento di Matematica e Fisica, Università del Salento, Lecce, Italy
- ^{68a}INFN Sezione di Milano, Milan, Italy
- ^{68b}Dipartimento di Fisica, Università di Milano, Milan, Italy
- ^{69a}INFN Sezione di Napoli, Napoli, Italy
- ^{69b}Dipartimento di Fisica, Università di Napoli, Napoli, Italy
- ^{70a}INFN Sezione di Pavia, Pavia, Italy
- ^{70b}Dipartimento di Fisica, Università di Pavia, Pavia, Italy
- ^{71a}INFN Sezione di Pisa, Pisa, Italy
- ^{71b}Dipartimento di Fisica E. Fermi, Università di Pisa, Pisa, Italy
- ^{72a}INFN Sezione di Roma, Rome, Italy
- ^{72b}Dipartimento di Fisica, Sapienza Università di Roma, Rome, Italy
- ^{73a}INFN Sezione di Roma Tor Vergata, Rome, Italy
- ^{73b}Dipartimento di Fisica, Università di Roma Tor Vergata, Rome, Italy
- ^{74a}INFN Sezione di Roma Tre, Rome, Italy
- ^{74b}Dipartimento di Matematica e Fisica, Università Roma Tre, Rome, Italy
- ^{75a}INFN-TIFPA, Trento, Italy
- ^{75b}Università degli Studi di Trento, Trento, Italy
- ⁷⁶Institut für Astro- und Teilchenphysik, Leopold-Franzens-Universität, Innsbruck, Austria
- ⁷⁷University of Iowa, Iowa City, Iowa, USA
- ⁷⁸Department of Physics and Astronomy, Iowa State University, Ames, Iowa, USA
- ⁷⁹Joint Institute for Nuclear Research, Dubna, Russia

- ^{80a}*Departamento de Engenharia Elétrica, Universidade Federal de Juiz de Fora (UFJF), Juiz de Fora, Brazil*
- ^{80b}*Universidade Federal do Rio De Janeiro COPPE/EE/IF, Rio de Janeiro, Brazil*
- ^{80c}*Universidade Federal de São João del Rei (UFSJ), São João del Rei, Brazil*
- ^{80d}*Instituto de Física, Universidade de São Paulo, São Paulo, Brazil*
- ⁸¹*KEK, High Energy Accelerator Research Organization, Tsukuba, Japan*
- ⁸²*Graduate School of Science, Kobe University, Kobe, Japan*
- ^{83a}*AGH University of Science and Technology, Faculty of Physics and Applied Computer Science, Krakow, Poland*
- ^{83b}*Marian Smoluchowski Institute of Physics, Jagiellonian University, Krakow, Poland*
- ⁸⁴*Institute of Nuclear Physics Polish Academy of Sciences, Krakow, Poland*
- ⁸⁵*Faculty of Science, Kyoto University, Kyoto, Japan*
- ⁸⁶*Kyoto University of Education, Kyoto, Japan*
- ⁸⁷*Research Center for Advanced Particle Physics and Department of Physics, Kyushu University, Fukuoka, Japan*
- ⁸⁸*Instituto de Física La Plata, Universidad Nacional de La Plata and CONICET, La Plata, Argentina*
- ⁸⁹*Physics Department, Lancaster University, Lancaster, United Kingdom*
- ⁹⁰*Oliver Lodge Laboratory, University of Liverpool, Liverpool, United Kingdom*
- ⁹¹*Department of Experimental Particle Physics, Jožef Stefan Institute and Department of Physics, University of Ljubljana, Ljubljana, Slovenia*
- ⁹²*School of Physics and Astronomy, Queen Mary University of London, London, United Kingdom*
- ⁹³*Department of Physics, Royal Holloway University of London, Egham, United Kingdom*
- ⁹⁴*Department of Physics and Astronomy, University College London, London, United Kingdom*
- ⁹⁵*Louisiana Tech University, Ruston, Louisiana, USA*
- ⁹⁶*Fysiska institutionen, Lunds universitet, Lund, Sweden*
- ⁹⁷*Centre de Calcul de l'Institut National de Physique Nucléaire et de Physique des Particules (IN2P3), Villeurbanne, France*
- ⁹⁸*Departamento de Física Teórica C-15 and CIAFF, Universidad Autónoma de Madrid, Madrid, Spain*
- ⁹⁹*Institut für Physik, Universität Mainz, Mainz, Germany*
- ¹⁰⁰*School of Physics and Astronomy, University of Manchester, Manchester, United Kingdom*
- ¹⁰¹*CPPM, Aix-Marseille Université, CNRS/IN2P3, Marseille, France*
- ¹⁰²*Department of Physics, University of Massachusetts, Amherst, Massachusetts, USA*
- ¹⁰³*Department of Physics, McGill University, Montreal, Quebec, Canada*
- ¹⁰⁴*School of Physics, University of Melbourne, Victoria, Australia*
- ¹⁰⁵*Department of Physics, University of Michigan, Ann Arbor, Michigan, USA*
- ¹⁰⁶*Department of Physics and Astronomy, Michigan State University, East Lansing, Michigan, USA*
- ¹⁰⁷*B. I. Stepanov Institute of Physics, National Academy of Sciences of Belarus, Minsk, Belarus*
- ¹⁰⁸*Research Institute for Nuclear Problems of Byelorussian State University, Minsk, Belarus*
- ¹⁰⁹*Group of Particle Physics, University of Montreal, Montreal, Quebec, Canada*
- ¹¹⁰*P. N. Lebedev Physical Institute of the Russian Academy of Sciences, Moscow, Russia*
- ¹¹¹*Institute for Theoretical and Experimental Physics of the National Research Centre Kurchatov Institute, Moscow, Russia*
- ¹¹²*National Research Nuclear University MEPhI, Moscow, Russia*
- ¹¹³*D. V. Skobel'syn Institute of Nuclear Physics, M. V. Lomonosov Moscow State University, Moscow, Russia*
- ¹¹⁴*Fakultät für Physik, Ludwig-Maximilians-Universität München, München, Germany*
- ¹¹⁵*Max-Planck-Institut für Physik (Werner-Heisenberg-Institut), München, Germany*
- ¹¹⁶*Nagasaki Institute of Applied Science, Nagasaki, Japan*
- ¹¹⁷*Graduate School of Science and Kobayashi-Maskawa Institute, Nagoya University, Nagoya, Japan*
- ¹¹⁸*Department of Physics and Astronomy, University of New Mexico, Albuquerque, New Mexico, USA*
- ¹¹⁹*Institute for Mathematics, Astrophysics and Particle Physics, Radboud University Nijmegen/Nikhef, Nijmegen, Netherlands*
- ¹²⁰*Nikhef National Institute for Subatomic Physics and University of Amsterdam, Amsterdam, Netherlands*
- ¹²¹*Department of Physics, Northern Illinois University, DeKalb, Illinois, USA*
- ^{122a}*Budker Institute of Nuclear Physics and NSU, SB RAS, Novosibirsk, Russia*
- ^{122b}*Novosibirsk State University, Novosibirsk, Russia*
- ¹²³*Institute for High Energy Physics of the National Research Centre Kurchatov Institute, Protvino, Russia*
- ¹²⁴*Department of Physics, New York University, New York, New York, USA*
- ¹²⁵*Ochanomizu University, Otsuka, Bunkyo-ku, Tokyo, Japan*
- ¹²⁶*Ohio State University, Columbus, Ohio, USA*
- ¹²⁷*Faculty of Science, Okayama University, Okayama, Japan*
- ¹²⁸*Homer L. Dodge Department of Physics and Astronomy, University of Oklahoma, Norman, Oklahoma, USA*
- ¹²⁹*Department of Physics, Oklahoma State University, Stillwater, Oklahoma, USA*
- ¹³⁰*Palacký University, RCPTM, Joint Laboratory of Optics, Olomouc, Czech Republic*
- ¹³¹*Center for High Energy Physics, University of Oregon, Eugene, Oregon, USA*
- ¹³²*LAL, Université Paris-Sud, CNRS/IN2P3, Université Paris-Saclay, Orsay, France*
- ¹³³*Graduate School of Science, Osaka University, Osaka, Japan*

- ¹³⁴*Department of Physics, University of Oslo, Oslo, Norway*
- ¹³⁵*Department of Physics, Oxford University, Oxford, United Kingdom*
- ¹³⁶*LPNHE, Sorbonne Université, Université de Paris, CNRS/IN2P3, Paris, France*
- ¹³⁷*Department of Physics, University of Pennsylvania, Philadelphia, Pennsylvania, USA*
- ¹³⁸*Konstantinov Nuclear Physics Institute of National Research Centre “Kurchatov Institute”, PNPI, St. Petersburg, Russia*
- ¹³⁹*Department of Physics and Astronomy, University of Pittsburgh, Pittsburgh, Pennsylvania, USA*
- ^{140a}*Laboratório de Instrumentação e Física Experimental de Partículas (LIP), Lisbon, Portugal*
- ^{140b}*Departamento de Física, Faculdade de Ciências, Universidade de Lisboa, Lisbon, Portugal*
- ^{140c}*Departamento de Física, Universidade de Coimbra, Coimbra, Portugal*
- ^{140d}*Centro de Física Nuclear da Universidade de Lisboa, Lisbon, Portugal*
- ^{140e}*Departamento de Física, Universidade do Minho, Braga, Portugal*
- ^{140f}*Universidad de Granada, Granada, Spain*
- ^{140g}*Dep Física and CEFITEC of Faculdade de Ciências e Tecnologia, Universidade Nova de Lisboa, Caparica, Portugal*
- ^{140h}*Av. Rovisco Pais, 1 1049-001 Lisbon, Portugal*
- ¹⁴¹*Institute of Physics of the Czech Academy of Sciences, Prague, Czech Republic*
- ¹⁴²*Czech Technical University in Prague, Prague, Czech Republic*
- ¹⁴³*Charles University, Faculty of Mathematics and Physics, Prague, Czech Republic*
- ¹⁴⁴*Particle Physics Department, Rutherford Appleton Laboratory, Didcot, United Kingdom*
- ¹⁴⁵*IRFU, CEA, Université Paris-Saclay, Gif-sur-Yvette, France*
- ¹⁴⁶*Santa Cruz Institute for Particle Physics, University of California Santa Cruz, Santa Cruz, California, USA*
- ^{147a}*Departamento de Física, Pontificia Universidad Católica de Chile, Santiago, Chile*
- ^{147b}*Departamento de Física, Universidad Técnica Federico Santa María, Valparaíso, Chile*
- ¹⁴⁸*Department of Physics, University of Washington, Seattle, Washington, USA*
- ¹⁴⁹*Department of Physics and Astronomy, University of Sheffield, Sheffield, United Kingdom*
- ¹⁵⁰*Department of Physics, Shinshu University, Nagano, Japan*
- ¹⁵¹*Department Physik, Universität Siegen, Siegen, Germany*
- ¹⁵²*Department of Physics, Simon Fraser University, Burnaby, British Columbia, Canada*
- ¹⁵³*SLAC National Accelerator Laboratory, Stanford, California, USA*
- ¹⁵⁴*Physics Department, Royal Institute of Technology, Stockholm, Sweden*
- ¹⁵⁵*Departments of Physics and Astronomy, Stony Brook University, Stony Brook, New York, USA*
- ¹⁵⁶*Department of Physics and Astronomy, University of Sussex, Brighton, United Kingdom*
- ¹⁵⁷*School of Physics, University of Sydney, Sydney, Australia*
- ¹⁵⁸*Institute of Physics, Academia Sinica, Taipei, Taiwan.*
- ^{159a}*E. Andronikashvili Institute of Physics, Iv. Javakhishvili Tbilisi State University, Tbilisi, Georgia*
- ^{159b}*High Energy Physics Institute, Tbilisi State University, Tbilisi, Georgia*
- ¹⁶⁰*Department of Physics, Technion, Israel Institute of Technology, Haifa, Israel*
- ¹⁶¹*Raymond and Beverly Sackler School of Physics and Astronomy, Tel Aviv University, Tel Aviv, Israel*
- ¹⁶²*Department of Physics, Aristotle University of Thessaloniki, Thessaloniki, Greece*
- ¹⁶³*International Center for Elementary Particle Physics and Department of Physics, University of Tokyo, Tokyo, Japan*
- ¹⁶⁴*Graduate School of Science and Technology, Tokyo Metropolitan University, Tokyo, Japan*
- ¹⁶⁵*Department of Physics, Tokyo Institute of Technology, Tokyo, Japan*
- ¹⁶⁶*Tomsk State University, Tomsk, Russia*
- ¹⁶⁷*Department of Physics, University of Toronto, Toronto, Ontario, Canada*
- ^{168a}*TRIUMF, Vancouver, British Columbia, Canada*
- ^{168b}*Department of Physics and Astronomy, York University, Toronto, Ontario, Canada*
- ¹⁶⁹*Division of Physics and Tomonaga Center for the History of the Universe, Faculty of Pure and Applied Sciences, University of Tsukuba, Tsukuba, Japan*
- ¹⁷⁰*Department of Physics and Astronomy, Tufts University, Medford, Massachusetts, USA*
- ¹⁷¹*Department of Physics and Astronomy, University of California Irvine, Irvine, California, USA*
- ¹⁷²*Department of Physics and Astronomy, University of Uppsala, Uppsala, Sweden*
- ¹⁷³*Department of Physics, University of Illinois, Urbana, Illinois, USA*
- ¹⁷⁴*Instituto de Física Corpuscular (IFIC), Centro Mixto Universidad de Valencia-CSIC, Valencia, Spain*
- ¹⁷⁵*Department of Physics, University of British Columbia, Vancouver, British Columbia, Canada*
- ¹⁷⁶*Department of Physics and Astronomy, University of Victoria, Victoria, British Columbia, Canada*
- ¹⁷⁷*Fakultät für Physik und Astronomie, Julius-Maximilians-Universität Würzburg, Würzburg, Germany*
- ¹⁷⁸*Department of Physics, University of Warwick, Coventry, United Kingdom*
- ¹⁷⁹*Waseda University, Tokyo, Japan*
- ¹⁸⁰*Department of Particle Physics, Weizmann Institute of Science, Rehovot, Israel*
- ¹⁸¹*Department of Physics, University of Wisconsin, Madison, Wisconsin, USA*

¹⁸²*Fakultät für Mathematik und Naturwissenschaften, Fachgruppe Physik, Bergische Universität Wuppertal, Wuppertal, Germany*

¹⁸³*Department of Physics, Yale University, New Haven, Connecticut, USA*

¹⁸⁴*Yerevan Physics Institute, Yerevan, Armenia*

^aAlso at Borough of Manhattan Community College, City University of New York, New York, New York, USA.

^bAlso at CERN, Geneva, Switzerland.

^cAlso at CPPM, Aix-Marseille Université, CNRS/IN2P3, Marseille, France.

^dAlso at Département de Physique Nucléaire et Corpusculaire, Université de Genève, Geneva, Switzerland.

^eAlso at Departament de Física de la Universitat Autònoma de Barcelona, Barcelona, Spain.

^fAlso at Departamento de Física, Instituto Superior Técnico, Universidade de Lisboa, Lisboa, Portugal.

^gAlso at Department of Applied Physics and Astronomy, University of Sharjah, Sharjah, United Arab Emirates.

^hAlso at Department of Financial and Management Engineering, University of the Aegean, Chios, Greece.

ⁱAlso at Department of Physics and Astronomy, Michigan State University, East Lansing, Michigan, USA.

^jAlso at Department of Physics and Astronomy, University of Louisville, Louisville, Kentucky, USA.

^kAlso at Department of Physics, Ben Gurion University of the Negev, Beer Sheva, Israel.

^lAlso at Department of Physics, California State University, East Bay, California, USA.

^mAlso at Department of Physics, California State University, Fresno, California, USA.

ⁿAlso at Department of Physics, California State University, Sacramento, California, USA.

^oAlso at Department of Physics, King's College London, London, United Kingdom.

^pAlso at Department of Physics, St. Petersburg State Polytechnical University, St. Petersburg, Russia.

^qAlso at Department of Physics, Stanford University, Stanford, California, USA.

^rAlso at Department of Physics, University of Adelaide, Adelaide, Australia.

^sAlso at Department of Physics, University of Fribourg, Fribourg, Switzerland.

^tAlso at Department of Physics, University of Michigan, Ann Arbor, Michigan, USA.

^uAlso at Dipartimento di Matematica, Informatica e Fisica, Università di Udine, Udine, Italy.

^vAlso at Faculty of Physics, M.V. Lomonosov Moscow State University, Moscow, Russia.

^wAlso at Giresun University, Faculty of Engineering, Giresun, Turkey.

^xAlso at Graduate School of Science, Osaka University, Osaka, Japan.

^yAlso at Hellenic Open University, Patras, Greece.

^zAlso at Institutio Catalana de Recerca i Estudis Avancats, ICREA, Barcelona, Spain.

^{aa}Also at Institut für Experimentalphysik, Universität Hamburg, Hamburg, Germany.

^{ab}Also at Institute for Mathematics, Astrophysics and Particle Physics, Radboud University Nijmegen/Nikhef, Nijmegen, Netherlands.

^{ac}Also at Institute for Nuclear Research and Nuclear Energy (INRNE) of the Bulgarian Academy of Sciences, Sofia, Bulgaria.

^{ad}Also at Institute for Particle and Nuclear Physics, Wigner Research Centre for Physics, Budapest, Hungary.

^{ae}Also at Institute of Particle Physics (IPP), Vancouver, Canada.

^{af}Also at Institute of Physics, Academia Sinica, Taipei, Taiwan.

^{ag}Also at Institute of Physics, Azerbaijan Academy of Sciences, Baku, Azerbaijan.

^{ah}Also at Institute of Theoretical Physics, Ilija State University, Tbilisi, Georgia.

^{ai}Also at Instituto de Física Teórica, IFT-UAM/CSIC, Madrid, Spain.

^{aj}Also at Joint Institute for Nuclear Research, Dubna, Russia.

^{ak}Also at LAL, Université Paris-Sud, CNRS/IN2P3, Université Paris-Saclay, Orsay, France.

^{al}Also at Louisiana Tech University, Ruston, Louisiana, USA.

^{am}Also at LPNHE, Sorbonne Université, Université de Paris, CNRS/IN2P3, Paris, France.

^{an}Also at Manhattan College, New York, New York, USA.

^{ao}Also at Moscow Institute of Physics and Technology State University, Dolgoprudny, Russia.

^{ap}Also at National Research Nuclear University MEPhI, Moscow, Russia.

^{aq}Also at Physics Department, An-Najah National University, Nablus, Palestine.

^{ar}Also at Physics Department, University of South Africa, Pretoria, South Africa.

^{as}Also at Physikalisches Institut, Albert-Ludwigs-Universität Freiburg, Freiburg, Germany.

^{at}Also at School of Physics, Sun Yat-sen University, Guangzhou, China.

^{au}Also at The City College of New York, New York, New York, USA.

^{av}Also at The Collaborative Innovation Center of Quantum Matter (CICQM), Beijing, China.

^{aw}Also at Tomsk State University, Tomsk, and Moscow Institute of Physics and Technology State University, Dolgoprudny, Russia.

^{ax}Also at TRIUMF, Vancouver, British Columbia, Canada.

^{ay}Also at Università di Napoli Parthenope, Napoli, Italy.

*Deceased.